Anion-Exchange Membrane Water Electrolysis: Synergistic Advances from Material Design to Device Integration

Yu Sun[1], Zhengxi Zhao[1], Ziqi Wang[1], Yanping Guo[1], Hengqi Liu[1,*], Depeng Zhao[1,*] and Xiang Wu[2,*]

[1]*School of New Energy, Shenyang Institute of Engineering, Shenyang, Liaoning, CN 110136, P. R. China*

[2]*School of Materials Science and Engineering, Shenyang University of Technology, Shenyang 110870, PR China*

Abstract: In the context of the global energy transition, wind and solar power have emerged as the primary sources of renewable energy. However, due to their reliance on natural conditions, their electricity generation is subject to fluctuations and intermittency, making large-scale and high-proportion grid integration challenging. This often results in surplus electricity. Hydrogen production through water electrolysis using this excess electricity plays a critical role in improving energy utilization efficiency. Among various water electrolysis technologies, anion exchange membrane water electrolysis (AEMWE) stands out as one of the most promising and cost-effective methods, owing to its high efficiency, the use of non-precious metal electrocatalysts, and extensive research. This paper reviews the recent advancements in the AEMWE field, highlighting improvements in membrane conductivity, a deeper understanding of degradation mechanisms, and emerging trends in electrocatalyst design. It systematically examines the key factors influencing AEMWE performance and explores the technological challenges and opportunities for its development. Finally, the paper offers valuable insights for the development of efficient and durable electrocatalysts and the advancement of AEMWE device fabrication.

Keywords: Electrocatalysis, Anion exchange membrane, Water dissociation, Oxygen evolution reaction, Hydrogen evolution reaction.

INTRODUCTION

The global transition to clean energy is accelerating; installed capacity and generation from wind and solar are projected to grow substantially [1, 2]. In the near term, renewables are expected to supply a much larger share of global electricity, becoming a cornerstone of sustainable energy systems [3]. Against this backdrop, advances in electrochemical technologies are closely coupled to power-sector transformation. In particular, electrochemical energy-conversion routes such as water electrolysis for hydrogen-a key step in the power-to-hydrogen pathway-are assuming an increasingly important role [4]. Converting surplus wind and photovoltaic electricity to green hydrogen can ease grid-integration constraints. Owing to its high specific energy (~140 MJ kg^{-1}) and the potential for zero carbon emissions when produced from renewable electricity, hydrogen is among the most sustainable media for long-duration energy storage [5]. Water electrolysis therefore enables the production of green hydrogen from renewable power with high efficiency and no direct carbon emissions. The principal technological routes are alkaline water electrolysis (AWE), proton-exchange-membrane water electrolysis (PEMWE), solid-oxide electrolysis cells (SOECs), and anion-exchange-membrane water electrolysis (AEMWE), each with distinct advantages and limitations [6-10]. SOECs currently deliver high efficiency but require elevated operating temperatures (700-1000°C) [11]. Eight-mol% Y_2O_3-doped ZrO_2 (8YSZ) is the most widely used solid-oxide electrolyte owing to its high oxide-ion conductivity at elevated temperature, which enables fast ion transport and low ohmic losses. Because this conductivity is strongly temperature-dependent, efficient SOEC operation requires high temperatures. In addition, the product hydrogen stream typically requires further purification to achieve high purity. System complexity, reliance on external high-temperature heat, and associated manufacturing costs indicate that substantial research and development are still required to enable large-scale commercialization of SOEC.

Over the past several decades, substantial research and industrial investment have focused on optimizing PEMWE [12]. Solid polymer electrolytes with high proton conductivity (*e.g.*, Nafion) enable effective separation of product gases and reduce ohmic losses, thereby delivering high-efficiency, high-purity hydrogen production [13]. PEMWE systems also exhibit rapid dynamic response, compact architecture, and the ability to operate at elevated pressure and high current densities (up to 10 A cm^{-2}), while maintaining high efficiency and H_2 purity. However, reliance on noble-metal electrocatalysts and the high cost of

*Address correspondence to this author at the School of New Energy, Shenyang Institute of Engineering, Shenyang, Liaoning, CN 110136, P. R. China:
E-mail: liuhengqi@163.com; hellodepeng@163.com; wuxiang05@sut.edu.cn

Received on 07-10-2025 Accepted on 05-11-2025 Published on 06-11-2025

E-ISSN: 3110-9772/25

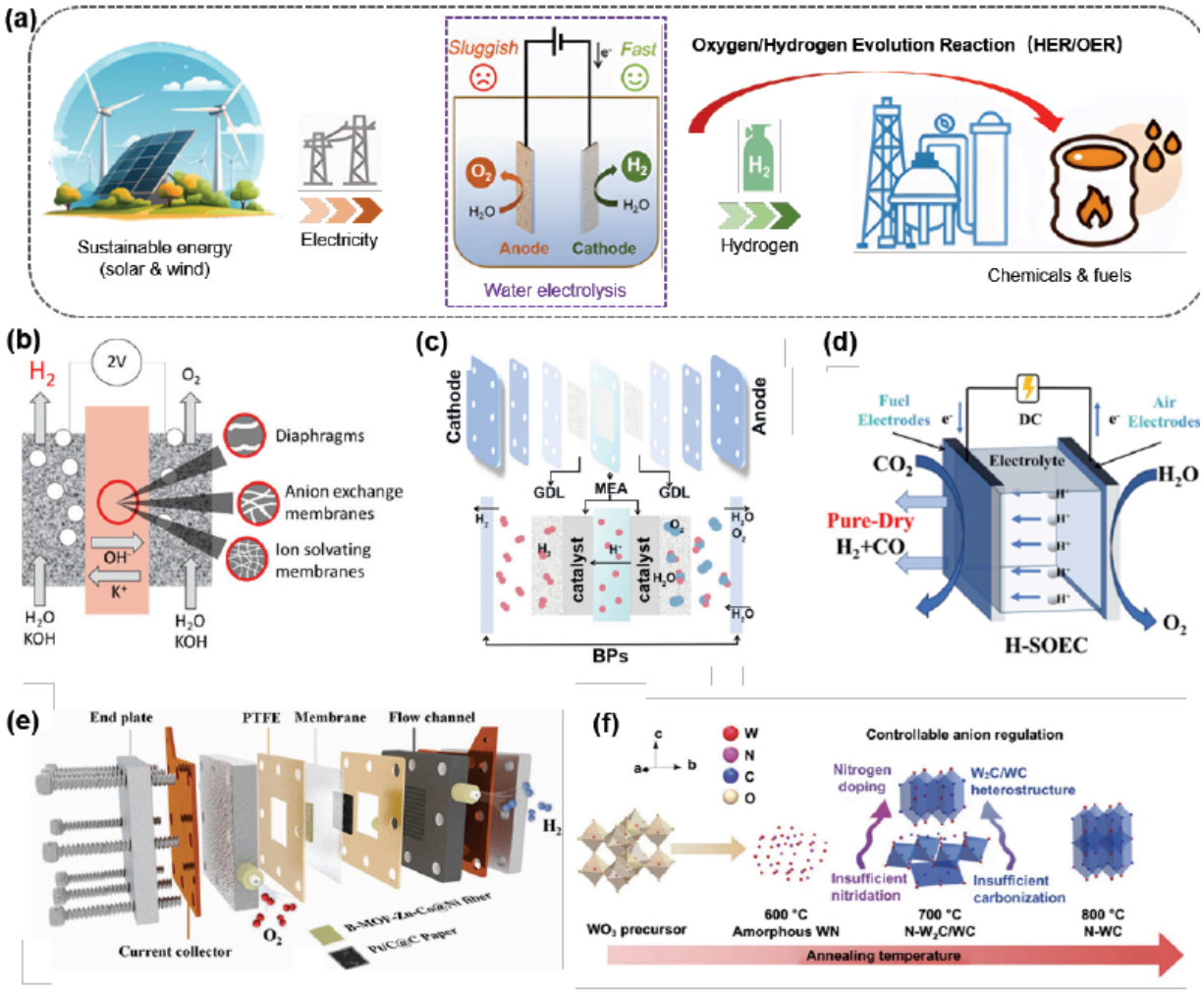

Figure 1: (**a**) Diagram of the Application of Sustainable Energy in Water Electrolysis.(**b**) Diagram illustrating the application of sustainable energy in water electrolysis, highlighting the use of diaphragms, anion exchange membranes, and ion solvation membranes. Reprinted with permission.[6] Copyright 2024, The Author(s). (**c**) Stack structure and the principle of a PEMWE. Reprinted with permission.[7] Copyright 2024, The Author(s). (**d**) Operating principle of H-SOEC. Reprinted with permission.[8] Copyright 2025, The Author(s). (**e**) Diagram of AEMWE device. Reprinted with permission.21 Copyright 2022 Elsevier B.V. (**f**) Schematic representation of the controllable anion regulation. Reprinted with permission.[22] Copyright 2022, The Author(s).

gas-diffusion layers and bipolar plates result in substantial upfront capital expenditure. Conventional AWE operates at relatively low temperatures (60-90 °C) with aqueous KOH and/or NaOH electrolytes [14]. Historically, asbestos diaphragms were used-now largely replaced by PPS or composite membranes-and electrodes are primarily Ni-based. Maximum geometric current densities are typically<0.4Acm^{-2};specific energy consumption for hydrogen production is 4.5-5.5 kWh Nm^{-3}, corresponding to an overall energy efficiency of 60% [15]. Despite its technological maturity and low materials cost, AWE faces persistent bottlenecks-low operating current densities, moderate gas purity, and limited dynamic response-that limit its suitability for high-efficiency, flexible hydrogen production.

Relative to conventional AWE, AEMWE retains the benefits of non-precious-metal catalysts and low materials cost. By replacing the liquid electrolyte and diaphragm with a dense anion-exchange membrane, it improves ionic selectivity and suppresses gas crossover, thereby significantly enhancing hydrogen purity [16]. AEMWE can operate at higher current densities (>1 A cm^{-2}), which reduces ohmic losses, improves energy efficiency, and enables faster dynamic response. These attributes make AEMWE well suited to the variable output of renewable power, combining the economics of AWE with selected high-performance attributes of PEMWE [17]. Nonetheless, large-scale deployment requires addressing key challenges, notably long-term durability and reliable operation at high current density [18]. Consequently, developing higher-performance,

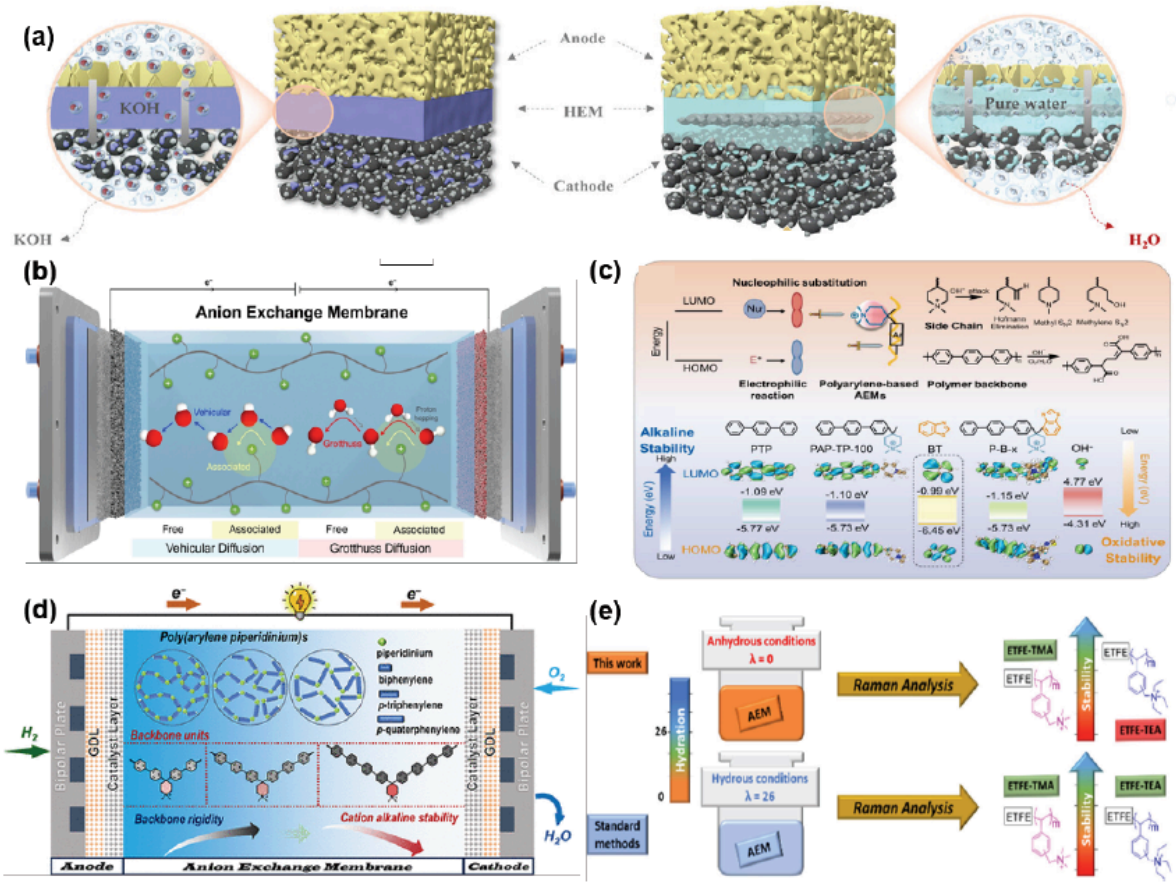

Figure 2: (**a**) Conventional HEMs (Tg > 200 °C) in MEA with KOH supporting electrolyte and QPS-x%-R-PEEK (Tg<100 °C) in MEA for pure water-fed HEMEL.Reprinted with permission.[32] Copyright 2025 Wiley-VCH GmbH. (**b**) Schematic illustration of the different diffusion mechanisms of hydroxide in nanopores of anion exchange membranes (AEMs). Reprinted with permission .[40] Copyright 2024 Wiley-VCH GmbH. (**c**) Correlation between frontier molecular orbital engineering and AEM stability and chemical stability of model compounds and BT with calculated LUMO and HOMO energies. Reprinted with permission .[42] Copyright 2025 Wiley-VCH GmbH. (**d**) The impact of polymer backbone rigidity on the alkaline stability of poly(arylene piperidinium) anion-exchange membranes. Reprinted with permission.[43]Copyright 2025, American Chemical Society. (**e**) Comparison of Raman analysis under anhydrous (λ = 0) and hydrated (λ = 26) conditions for poly(arylene piperidinium) anion-exchange membranes (AEMs). Reprinted with permission.[47] Copyright 2023 American Chemical Society.

lower-cost electrocatalysts and anion-exchange membranes (AEMs) remains a central research priority for AEM water electrolysis.

The device has a typical sandwich architecture comprising an anion-exchange membrane (AEM), electrocatalyst layers for the oxygen evolution reaction (OER) and the hydrogen evolution reaction (HER), gas-diffusion layers (GDLs), current collectors, and end plates [19]. In practical realizations, the sandwich is configured in a zero-gap assembly in which the porous transport/GDL elements are pressed directly against the catalyst-coated membrane to minimize interfacial contact resistance; the flow fields etched or machined into the current collectors (*e.g.*, serpentine, interdigitated, or parallel channels) distribute liquid, manage two-phase flow, and facilitate removal of product gases while maintaining uniform compression across the active area. The basic operating principle of an AEM water electrolyzer is shown schematically in Figure **1**: under an applied cell voltage of 1.8-2.5 V, water is reduced at the cathode via the HER to produce H_2, while the AEM separates the electrodes to prevent H_2-O_2 mixing; oxygen is generated at the anode via the OER [20]. Under typical operating conditions (40-80 °C; ambient to elevated pressure on the H_2 side), electrolyte is circulated to the anode to sustain the OER and maintain membrane hydration; cathode operation may use either pure water or dilute alkaline feed depending on stack design and materials compatibility. Under the applied bias, electrons reach active sites on the cathode catalyst, where the HER produces H_2 and hydroxide ions (OH^-). In alkaline media this proceeds through the Volmer step ($H_2O + e^- \rightarrow H^* + OH^-$) followed by either Heyrovsky ($H^* + H_2O + e^- \rightarrow H_2 + OH^-$) or Tafel ($H^* + H^* \rightarrow H_2$) pathways on Ni-based or alloy catalysts, with local wettability, pore architecture, and ionomer coverage governing the density of triple-phase boundaries and thus the apparent kinetics. The OH^- then migrates through the AEM from the cathode to the anode and participates in the OER on the anode catalyst surface, forming

surface-bound OH and OOH intermediates and thereby completing the ionic conduction cycle [21]. On Ni-Fe oxyhydroxide-type OER catalysts, the adsorbate-evolution mechanism is often invoked, though lattice-oxygen participation can emerge under aggressive conditions; in all cases, anode porosity, bubble dynamics, and channel shear influence concentration overpotentials and gas crossover tendencies. Consequently, coordinated optimization of mass transport, electron conduction, electrode kinetics, and thermal management within the cell dictates overall electrolyzer efficiency and is critical to increasing hydrogen production rates and energy efficiency in AEMWE. In particular, ohmic losses are governed by AEM thickness/ionic conductivity and by interfacial contact resistances; kinetic losses depend on intrinsic catalyst activity and ionomer–catalyst interactions; and mass-transport losses reflect water delivery, removal of two-phase mixtures, and suppression of H_2/O_2 crossover under differential pressure. Effective thermal management removes joule and reaction heat to stabilize membrane hydration and ionomer integrity, while manifold/flow-field design mitigates maldistribution and shunt currents at the stack level. Taken together, careful co-design of membrane/ionomer chemistry, catalyst layer microstructure (porosity, tortuosity, and wettability gradients), GDL/porous-transport selection, flow-field geometry, sealing and compression, and operating strategy (water feed location, temperature, pressure, and dynamic load profile) is essential to realize high current density at low cell voltage with durable performance in AEMWE.

The half-cell and overall reactions in AEMWE are as follows [22]:

$$4OH^- \rightarrow O_2 + 4e^- + 2H_2O \ (E_0 = 0.401\ V) \quad (1);$$

$$4H_2O + 4e^- \rightarrow 2H_2 + 4OH^- \ (E_0 = 0.828\ V) \quad (2);$$

$$4H_2O \rightarrow 2H_2 + O_2 \ (E_0 = 1.23\ V) \quad (3).$$

According to these reactions, the cathodic HER involves water dissociation to form an adsorbed hydrogen intermediate (H*) and OH^-, a step that is kinetically sluggish in alkaline media and therefore incurs substantial overpotential. In alkaline electrolytes the Volmer step ($H_2O + e^- \rightarrow H^* + OH^-$) precedes either Heyrovsky (electrochemical desorption) or Tafel (recombination) and often becomes rate determining because the initial cleavage of the O–H bond requires additional activation and interfacial reorganization of hydrogen-bonded water; cation identity, local pH, double-layer structure, and interfacial water orientation further modulate barrier heights and apparent Tafel slopes by affecting OH^- stabilization and proton shuttling to the active site [23]. Although many HER catalysts perform well in acidic electrolytes, their performance under alkaline conditions remains limited, primarily because of insufficient active sites to stabilize adsorbed OH^- and promote water dissociation. To address this, effective alkaline-HER designs deploy bifunctional motifs that pair near-thermoneutral H*-binding sites with adjacent oxophilic centers (*e.g.*, NiMo/NiMoN, NiW, metal–hydroxide or metal–oxide heterointerfaces) to accelerate water adsorption/dissociation, while strain engineering, ligand effects, heteroatom doping, and defect creation tune electronic structure; at the electrode level, ionomer content, wettability control, and hierarchical porosity increase triple-phase boundary density and mitigate bubble blockage and local OH^- depletion, improving utilization at high current density [24, 25]. Meanwhile, the OER typically requires large overpotentials; its pathway entails multiple proton-electron-coupled transfer steps, and the detailed mechanism remains incompletely resolved. On NiFe-based oxyhydroxides and related transition-metal (oxy)hydroxides/spinels, an adsorbate-evolution sequence (*OH → *O → *OOH → O_2) is commonly invoked, though lattice-oxygen participation can emerge under aggressive conditions; universal scaling between *OH, *O, and *OOH adsorption energies imposes a thermodynamic floor on the overpotential, while coverage-dependent kinetics, electrolyte composition (including carbonate/bicarbonate), and operating temperature/pressure shift the rate-determining step and stability window [26, 27]. The theoretical reversible cell voltage of 1.23 V is set by the Gibbs free energy (ΔG) of water splitting under standard conditions [28, 29]. In practice, however, the operating voltage of AEMWE devices is considerably higher, mainly owing to kinetic overpotentials at the electrodes and resistive losses within the cell [30]. Therefore, developing AEMs with high hydroxide conductivity together with bifunctional electrode materials that combine high electrocatalytic activity with durability is essential for reducing overall overpotential and improving energy-conversion efficiency.

2. STATUS OF ANION-EXCHANGE MEMBRANES

Anion-exchange membranes (AEMs) are core components of anion-exchange membrane water electrolyzers (AEMWE). Together with the oxygen-evolution reaction (OER) and hydrogen-evolution reaction (HER) catalyst layers, they form extended three-phase boundaries that improve electrode design and simplify gas management [31]. In practice, gas management entails that the AEM separates the H_2 and O_2 generated at the electrodes

and provides pathways for hydroxide (OH^-) and water transport. Beyond preventing bulk mixing, the membrane suppresses diffusive and pressure-driven crossover by combining low gas permeability with adequate thickness and mechanical integrity under compression; appropriate flow-field design and controlled hydration further limit bubble residence and local supersaturation. The membrane also provides electrical insulation, preventing direct electron conduction between electrodes, ensuring that current flows through the external circuit, and preserving electrochemical efficiency [32]. At the microscopic level, AEMs typically consist of a phase-separated polymer framework in which hydrophilic ionic clusters-formed by covalently tethered cationic groups (*e.g.*, quaternary ammonium)-aggregate into continuous OH^--conducting channels. In advanced designs, the polymer architecture (backbone chemistry, tether length, and cation identity) and processing (casting solvent, annealing, and crosslinking) are tuned to control ion-cluster size and connectivity, as evidenced by small-angle scattering signatures of well-defined domain spacings and by microscopy that reveals percolated water-rich pathways. This ion-cluster network is analogous to that in proton-exchange membranes (PEMs), except that OH^- rather than H^+ is the mobile charge carrier. Upon water uptake, swelling increases microphase separation, and OH^- migrates along the hydrophilic channels [33]. Because water uptake (often parameterized by hydration number λ and water-content-dependent ion-exchange capacity) simultaneously enhances ion mobility and risks excessive swelling, anisotropic expansion, and loss of mechanical strength, practical membranes employ reinforcement, judicious crosslink densities, and inorganic fillers to stabilize dimensional change while maintaining percolation. Hydroxide transport proceeds via Grotthuss, vehicle, and surface mechanisms, because structural diffusion is less efficient for OH^- than for H^+, OH^- mobility and thus AEM ionic conductivity-is generally lower than in PEMs. Typical AEMs therefore target high-through-plane conductivity at operating temperature while balancing electro-osmotic drag, back-diffusion, and water-management demands that otherwise foster local drying at the cathode or flooding at the anode. Operation in ambient environments further complicates transport: CO_2 uptake converts OH^- to carbonate, diminishing effective conductivity and altering water activity, so carbonate tolerance and mitigation strategies are integral to robust design. Moreover, at high pH and high potentials the cationic headgroups are susceptible to nucleophilic attack and Hofmann elimination, compromising chemical stability and creating a durability gap relative to PEMs [34]. Degradation pathways include SN2 displacement at benzylic sites, β-elimination at cations bearing accessible β-hydrogens, and oxidative damage from radical species generated at the anode; stabilization strategies consequently emphasize sterically shielded and elimination-resistant cations,aryl-ether–free or otherwise oxidation-resistant backbones, spacer engineering that decouples cation electronics from the main chain, and radical-scavenging or inorganic-filler additions. At the membrane-electrode interface, tailored ionomer distributions and strong interfacial adhesion minimize contact resistance and delamination under hydration/thermal cycling, while optimized thickness and reinforcement enable low ohmic loss without sacrificing gas-separation performance-collectively supporting high-current, low-voltage AEMWE operation with durable, efficient mass and charge transport.

Additionally, the AEM should be regarded as a functional thin film, whose performance in anion-exchange membrane water electrolysis is determined not only by its chemical composition, but also by the interplay among fabrication processes, nanoscale microstructure, and interfacial architecture. Typically fabricated via solution casting or blade-coating, the AEM undergoes solvent evaporation and self-assembly, forming a microphase-separated morphology in which hydrophilic ionic clusters create a percolated network that provides pathways for hydroxide ion conduction, while the hydrophobic polymer matrix ensures mechanical robustness and dimensional stability. This microstructure is highly sensitive to processing parameters such as polymer concentration, solvent selection, and drying kinetics, and directly governs key performance metrics including ionic conductivity, water uptake, and alkaline stability.

Accordingly, future AEM development should prioritize four attributes: high hydroxide-ion conductivity, strong alkaline and thermal stability, low swelling, and excellent mechanical robustness. Contemporary AEM designs are driven by the need for efficient, low-cost electrolytic hydrogen production, particularly in AEMWE systems [35]. To enable flexible hydrogen generation compatible with the intermittency of wind and solar power, the central challenge is to engineer membranes that combine high OH^- conductivity, outstanding chemical stability, and adequate mechanical strength, thereby delivering low ohmic losses, high gas purity, and long operational lifetimes.

(1). Conductivity of Anion-Exchange Membranes (AEMs)

Enhancing the conductivity of anion-exchange membranes (AEMs) is critical to the efficiency of anion-exchange membrane water electrolyzers

(AEMWE). Rational membrane design demands a clear understanding of anion-transport kinetics within the polymer. Increasing the ion-exchange capacity (IEC) is a common approach to boost conductivity because it facilitates OH^- transport; however, it often induces excessive water uptake, compromises mechanical strength, and causes dimensional instability [36]. Accordingly, state-of-the-art strategies emphasize decoupling ionic conductivity from uncontrolled swelling by (i) engineering ion-cluster morphology to maximize percolation and minimize tortuosity of OH^- pathways, (ii) tuning cation spacing and side-chain architecture to regulate local hydration (hydration number λ) and suppress counterion condensation, and (iii) introducing reinforcement and controlled crosslinking to provide an elastic restoring force without obstructing through-plane transport. At the molecular level, conductivity gains arise when well-connected hydrophilic domains host continuous hydrogen-bond networks that support parallel Grotthuss and vehicular OH^- migration; at the mesoscale, balanced water management limits cathode-side drying and anode-side flooding while preserving low gas permeability. From a mechanical perspective, membranes must sustain compressive loads in zero-gap assemblies and resist creep under differential pressure, motivating designs that combine high IEC with adequate tensile strength and dimensional stability. To mitigate these trade-offs, Zhu *et al*. developed a non-aromatic cationic monomer-bearing a piperidinium group tethered to an aliphatic chain-that leverages intermolecular interactions to regulate microphase separation while maintaining a moderate IEC, thereby achieving efficient ion transport (OH^- conductivity 126 mS cm^{-1} at 80 °C) and excellent chemical and mechanical stability [37]. In this construct, the sterically protected, elimination-resistant piperidinium cation enhances alkaline durability, the flexible aliphatic tether promotes cooperative hydration within ion clusters, and the moderated IEC curbs over-swelling-together yielding robust, low-resistance membranes suitable for high-current, low-voltage AEMWE operation.

A complementary strategy introduces flexible hydrophilic side chains into a rigid, hydrophobic backbone to increase segmental mobility and promote microphase separation into well-defined hydrophilic and hydrophobic domains. By lowering the glass transition temperature of the ionic phase and softening local chain dynamics around the tethered cations, these side chains facilitate self-assembly into percolated water-rich channels with reduced tortuosity. Such nanophase-separated morphologies create continuous hydrophilic networks that enhance OH^- transport; the connectivity and length scale of these pathways strongly influence ionic conductivity, with domain spacing and cluster–cluster correlation lengths (as evidenced by scattering signatures) correlating with through-plane conductivity and reduced *iR* losses under device-relevant compression [38]. Design levers include side-chain length, density, and polarity to tune local hydration number (λ) and mitigate counterion condensation, as well as anchoring geometry (pendant versus grafted) to control cation proximity and suppress ionic aggregation that can trap water without improving percolation. For example, incorporating flexible perfluorinated side chains into a poly(arylpiperidinium) backbone induces pronounced microphase separation and yields an OH^- conductivity of 115.5 mS cm^{-1} at 80°C.Additional molecular design tactics-including branched architectures, sterically bulky substituents, and intrinsically microporous backbones-are widely employed to increase fractional free volume (FFV), disrupt tight chain packing, and foster continuous hydrophilic channels that boost OH^- mobility [39]. In practice, these modifications must be balanced against swelling pressure, creep, and gas permeability: excessive side-chain content or FFV can elevate water uptake, reduce modulus, and increase H_2/O_2 crossover. Consequently, side-chain engineering is often paired with controlled crosslinking, reinforcement, and spacer/cation chemistries that resist β-elimination and nucleophilic displacement-thereby preserving mechanical integrity and alkaline stability while sustaining high conductivity and acceptable electro-osmotic drag. At the device level, such membranes support robust water management and carbonate tolerance, maintain low contact resistance to catalyst layers, and enable low-voltage, high-current AEMWE operation over dynamic load profiles.

Beyond structural design, recent work has focused on optimizing OH^- transport mechanisms in AEMs. Typically, OH^- migrates via two principal pathways: (i) the vehicle mechanism, wherein OH^- forms hydrated complexes (*e.g.*, $OH^-{\cdot}nH_2O$) that move with water clusters and therefore depend on adequate membrane hydration; and (ii) the Grotthuss mechanism, wherein OH^- is relayed through hydrogen-bond networks by site-to-site hopping between fixed hydrophilic sites (*e.g.*, cationic or polar groups). Because structural diffusion is inherently more efficient in the Grotthuss pathway, it provides higher mobility and lower activation energy, whereas vehicle transport slows under low-hydration conditions [40, 41]. In practical membranes, the relative contributions of these pathways are governed by water activity and the connectivity, tortuosity, and dimensional stability of hydrophilic channels; accordingly, maximizing continuous hydrogen-bond networks while suppressing

excessive swelling helps lower the apparent activation energy and sustain high through-plane conductivity under compression. From a transport-kinetics perspective, σ follows a Nernst-Einstein-type relation linking charge-carrier density and diffusivity, with deviations (Haven ratios) reflecting correlated hopping and ion pairing; temperature dependences often interpolate between Arrhenius behavior (for well-formed percolated pathways) and segmental-motion-coupled Vogel-Tammann-Fulcher trends (when polymer dynamics limit rearrangement of the hydrogen-bond network). Water management is therefore central: adequate hydration promotes Grotthuss relays without incurring undue electro-osmotic drag or gas crossover, while carbonate formation reduces effective OH^- mobility and must be mitigated to preserve low iRΩiR_Omega iRΩ losses at stack level. Building on these principles, Liu *et al*. combined frontier molecular-orbital (FMO) engineering with deliberate construction of hydrogen-bond networks, using the HOMO energy level as a descriptor of backbone oxidative stability and the LUMO level as an indicator of the alkaline stability of cationic sites. By aligning electronic structure with robust hydrogen-bond connectivity, the optimized AEM exhibited an OH^- conductivity of 168.7 ± 1.0 mS cm^{-1} at 80 °C and operated stably for more than 500 h at 1.0 A cm^{-2} in 1.0 mol L^{-1} KOH, with a voltage-decay rate of 32 μV h^{-1} [42].

External magnetic fields have also been explored to guide the formation or alignment of ion-transport channels. Another widely adopted approach is crosslinking of functional groups and/or the polymer backbone. For example, Li *et al*. introduced crosslinkable moieties (*e.g*., divinylbenzene) into the backbone and used UV^- or thermally initiated crosslinking to form three-dimensional (3D) network AEMs. This architecture effectively suppresses excessive swelling at high IEC while maintaining high OH^- conductivity (>100 mS cm^{-1} at 80 °C) and substantially enhancing alkaline stability (stable for ≥1000 h in 1 M NaOH at 80 °C).

(2). Degradation of Anion-Exchange Membranes (AEMs)

When operated in anion-exchange membrane water electrolyzers (AEMWE) and exposed to high-pH environments, AEMs often exhibit higher energy consumption and lower efficiency owing to membrane degradation. This degradation results from chemical cleavage of the polymer backbone and/or the cationic headgroups under alkaline conditions and high potentials, which diminishes ionic conductivity and mechanical integrity and ultimately leads to membrane failure. At the device level, progressive loss of ion-exchange capacity elevates area-specific resistance, increases cell voltage at a given current density, and exacerbates gas crossover as defects accumulate; simultaneous hydration fluctuations and compressive loads can accelerate crack initiation, creep, and interfacial delamination, further compounding ohmic and mass-transport losses. At the molecular level, hydroxide attacks cationic sites, inducing Hofmann elimination and loss of the cationic functionality, whereas the backbone undergoes base-promoted hydrolytic scission; additional pathways may be triggered under anodic conditions where reactive oxygen species and high local potentials promote oxidative chain damage and microstructural coarsening of ionic domains. The rates of these processes increase with temperature, hydroxide activity, and time at bias, reflecting Arrhenius-type kinetics and the sensitivity of interfacial microenvironments to water activity and carbonate formation. Accordingly, selecting robust functional groups and developing cationic chemistries with strong alkaline stability are effective means to suppress AEM degradation [43, 44]. In parallel, macromolecular designs that limit water-induced swelling while preserving percolated ion channels, controlled crosslinking and reinforcement to resist mechanical fatigue, and operating strategies that stabilize hydration and minimize impurity ingress can further reduce voltage growth and extend service life without sacrificing conductivity.

In AEMs, tethered cationic groups fix positive charge, attract OH^-, and organize hydrophilic channels; hydrogen-bond networks then facilitate site-to-site hopping or concerted transfer of hydroxide, enabling ion conduction. The spatial distribution and intrinsic stability of these groups are therefore key design variables for high-performance AEMs [45]. Pan *et al*. investigated polyxanthene (PX)-based AEMs. Using 4,4′-biphenylol and bromoalkylated trifluoroacetophenone monomers, they synthesized a PX precursor (PX-BR) via poly(hydroxyalkylation)-cyclodehydration. Subsequent Menschutkin quaternization of PX-BR with trimethylamine, methylpiperidine, or a “Qui” cation source yielded three quaternary-ammonium-functionalized polymers-PXTMA, PXmPip, and PXQui. Owing to its highest ion-exchange capacity (IEC), the PXTMA membrane exhibited an OH^- conductivity of 129 mS cm^{-1} at 80 °C; by contrast, PXQui showed superior alkaline stability, with no measurable ion loss and an intact backbone after treatment in 2 M NaOH at 90 °C for 720 h, indicating substantially mitigated degradation [46].

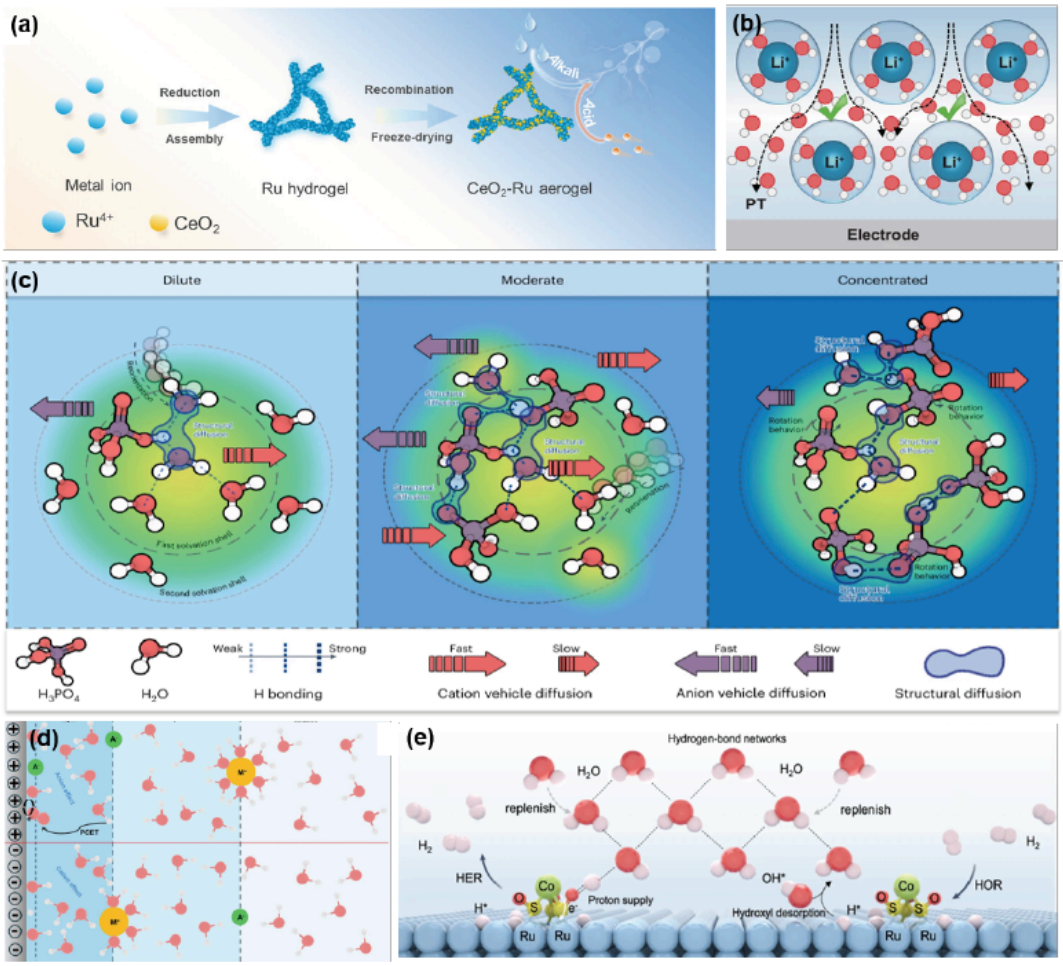

Figure 3: (**a**) Scheme illustration of the synthesis procedure of CeO_2-Ru aerogel. Reprinted with permission .[59] Copyright 2025 Wiley-VCH GmbH.(**b**) Schematic diagrams of the EDL structures at Pt(111)/$LiOH_{aq}$ interfaces and the proton transfer from bulk to interface through the H-bond network. Reprinted with permission.[61] Copyright 2025, The Author(s).(**c**) Schematic of H^+ transport behaviours in H_3PO_4 at various concentrations. Reprinted with permission.[63] Copyright 2025 Wiley-VCH GmbH.(**d**) Schematic diagram of the EDL at a positively charged interface. Overall model of the double layer showing solvent molecules, counterions, and specifically absorbed co-ions. Reprinted with permission.[64] Copyright 2019, The Author(s).(**e**) The schematic illustration of the dynamic hydrogen-bond network conformations. The dotted lines represent hydrogen bonds. Source data are provided as a Source Data file. Reprinted with permission.[65] Copyright 2025, The Author(s).

Historically, AEM stability has been benchmarked by immersing membranes in concentrated KOH (1-6 M) at elevated temperature and monitoring chemical decomposition. In operating AEMWE cells, however, the local cathodic environment differs: water consumption by the HER lowers water activity and effectively increases local hydroxide concentration and pH-conditions under which nucleophilic attack on cationic sites is most severe. These differences can compromise the rigor of comparisons, underscoring the need to control membrane water activity during testing. From a mechanistic standpoint, reduced water activity weakens hydroxide solvation, increases its effective nucleophilicity, and alters transition-state stabilization for SN2 displacement and β-elimination, thereby accelerating cation loss and backbone scission; simultaneously, gradients in hydration across the membrane thickness, local heat generation, and compressive stresses in zero-gap assemblies can couple to chemistry to produce heterogeneous degradation that conventional aqueous soak tests may not capture. To emulate the cathode's reduced water activity, Willdorf-Cohen *et al*. used a 0.5 M OH^-/DMSO medium and evaluated the alkaline stability of radiation-grafted AEMs (RG-AEMs; bearing BTMA or BTEA groups) and crosslinked AEMs (insoluble under non-extreme conditions). They tracked base-driven degradation kinetics by Raman and ATR-FTIR spectroscopy and corroborated the trends by monitoring changes in IEC and true OH^- conductivity, enabling quantitative extraction of degradation rates under well-defined activity, temperature, and time-at-bias conditions and establishing a test framework that is more representative of cathode-side microenvironments than conventional aqueous protocols [47].

Water activity in the cathode region is a key determinant of AEM chemical stability in AEMWE systems. During electrolysis, consumption of water

raises the local OH^- concentration, accelerating degradation of tethered cationic groups under *operando* conditions. Because water is also the reactant in the alkaline HER that generates H_2 and OH^-, concomitant OH^- formation and water depletion shift the local pH.

3. ELECTROCATALYSTS FOR THE ALKALINE HYDROGEN EVOLUTION REACTION (HER)

Under acidic conditions, the HER is typically described by two elementary steps with relatively fast kinetics. First, hydronium (H_3O^+) adsorbs at surface sites and is reduced to form adsorbed hydrogen (H*). Second, H_2 forms either by recombination of two H* (Tafel step) or by electrochemical desorption involving H* and H_3O^+ plus an electron (Heyrovsky step) [48]. In alkaline media, by contrast, water is the reactant: in the Volmer step, H_2O adsorbs and dissociates to furnish H* and OH^-. Consequently, cleavage of the O-H bond is required, and the overall kinetics are typically slower than in acid [49]. Theory and experiment support the following sequence (M denotes an active site) and characteristic Tafel slopes:

Volmer: $H_2O + M + e^- \rightarrow M–H^* + OH^-$ ($b \approx 120$ mV dec^{-1}) (4)

Heyrovsky: $M–H^* + H_2O + e^- \rightarrow H_2 + OH^- + M$ ($b \approx 40$ mV dec^{-1}) (5)

Tafel: $2M–H^* \rightarrow H_2 + 2M$ ($b \approx 30$ mV dec^{-1}) (6)

As in acidic media, alkaline HER can proceed through either the Volmer-Heyrovsky or Volmer-Tafel pathway [50, 51]. The key distinction is the identity of the reactant-H_3O^+ in acid versus H_2O in base-so catalysts must first cleave the H-OH bond to form H*. The rate of O-H-bond scission imposes an upper bound on the overall rate [52]. Accordingly, the alkaline HER is widely used as a model reaction for probing water-dissociation mechanisms. In alkaline media, the hydrogen evolution reaction is rate-limited by water dissociation in the Volmer step. Accordingly, catalyst design should (i) lower the Volmer barrier by juxtaposing oxophilic and metallic sites within ~2-3 nm and by controlling interfacial electric fields to orient water in the inner Helmholtz plane (IHP), and (ii) maintain a near-thermoneutral hydrogen-adsorption free energy (ΔG_{H^*}) to enable rapid recombination. In practice, site energetics can be tuned via alloying, lattice strain, and strong metal–support interactions (SMSI), whereas ionomer coverage, cation management, and hierarchical porosity together define the local electric double layer and the density of triple-phase boundaries. To ensure device-relevant gains, these levers should be validated in zero-gap membrane–electrode assemblies (MEAs) at ≥0.2-1 A cm^{-2} under differential pressure, with *operando* tracking of surface reconstruction and contact resistance.

Several frameworks rationalize the sluggish kinetics in alkaline electrolytes. (1) Hydrogen-binding energy (HBE) theory: an ideal HER catalyst exhibits a near-thermoneutral hydrogen adsorption free energy ($\Delta G_{H^*} \approx 0$); in base, many surfaces deviate from this optimum, hindering H adsorption/desorption and slowing the reaction [53]. (2) Water-dissociation theory**:** the initial step requires breaking the H-OH bond, which carries a substantial barrier and becomes rate-determining when catalysts do not promote dissociation [54]. (3) Potential of zero free charge (PZFC): near the PZFC, low surface charge density disfavors adsorption and activation of polar molecules, impeding water dissociation and subsequent proton-coupled electron transfer [55]. (4) “2B” framework (bifunctional + HSAB): high-performance catalysts provide bifunctional sites-metallic sites to adsorb/dissociate H_2O and basic/oxide sites to stabilize or shuttle OH^-; per hard-soft acid-base (HSAB) principles, soft acids (*e.g.*, Pt) prefer soft bases (H^*/H^-), while competitive adsorption of the hard base OH^- in alkaline media can suppress H* formation [56, 57].

Pt-based catalysts generally outperform earth-abundant alternatives for the HER, yet water dissociation still limits the maximum rate [58]. In alkaline media, the Volmer step (H_2O activation to form H*) imposes a substantial kinetic barrier such that even catalysts with near-ideal hydrogen-binding energetics cannot reach their intrinsic limit unless interfacial water cleavage is accelerated. Thanks to intensive recent efforts, non-precious composite catalysts have approached Pt-level performance. Progress has come from engineering bifunctional interfaces that couple oxophilic motifs for rapid H_2O adsorption/dissociation with conductive sites that afford near-thermoneutral H* binding and fast recombination, while concurrently tuning electronic structure, defect density, and strain to lower the activation enthalpy of the rate-determining step. Overall, catalyst design in alkaline media focuses on accelerating the rate-limiting water-dissociation step while maintaining near-optimal hydrogen binding. Complementary optimization of the catalyst-layer microenvironment-ionomer distribution, wettability, and hierarchical porosity-improves access to triple-phase boundaries, mitigates local OH^-depletion and bubble coverage, and preserves high utilization at practical current densities. Rigorous evaluation emphasizes intrinsic activity metrics (exchange current density, turnover frequency, Tafel slope) alongside durability under dynamic load, with attention to surface reconstruction, corrosion resistance, and adhesion

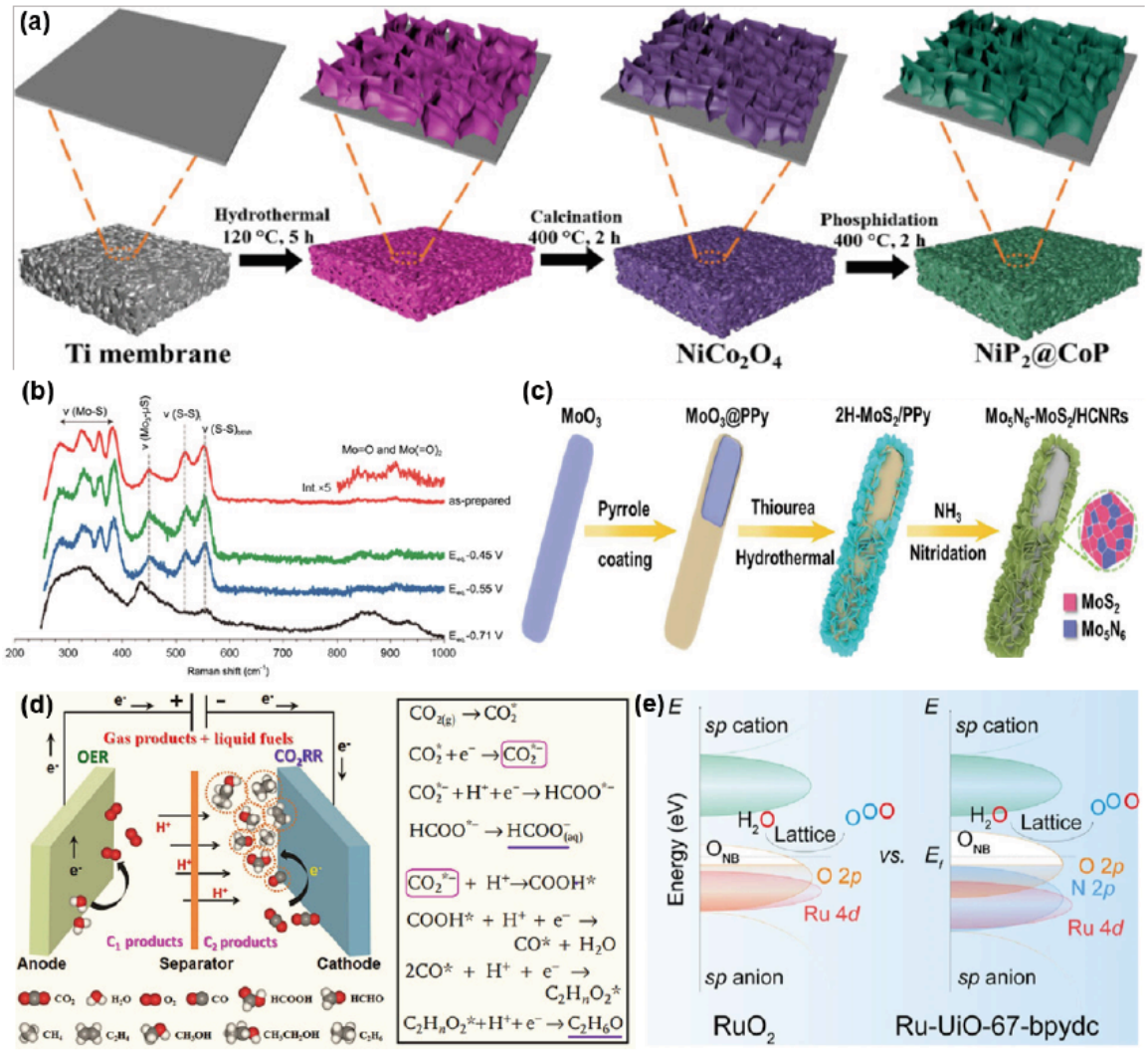

Figure 4: (**a**) Schematic illustration of the synthesis procedure for the NiP_2 @CoP catalyst. Reprinted with permission.[68] Copyright 2025 Elsevier Ltd.(**b**) Resonance Raman spectra of a-MoS_x catalysts. Reprinted with permission.[69] Copyright 2024, The Author(s).(**c**) Schematic illustration of the preparation procedures of the Mo_5N_6-MoS_2/HCNRs from the precursor of MoO_3 nanoribbons. Reprinted with permission.[70] Copyright 2022 Wiley-VCH GmbH.(**d**) Schematic diagram of CO_2RR process and the possible products. Reprinted with permission.[72] Copyright 2022 Hydrogen Energy Publications LLC.(**e**) Increased covalency of the Ru–O bond lowers the energy barrier for the lattice oxygen oxidation mechanism pathway. Reprinted with permission.[74] Copyright 2023, The Author(s).

within zero-gap architectures. When integrated with low-resistance membranes and minimized contact losses, these design principles reduce overpotential at target currents and translate materials-level gains into stack-level efficiency improvements in AEMWE

(1). Water Dissociation

There is broad agreement that, in alkaline HER, the Volmer step within the three-step mechanism directly or indirectly limits the overall rate [59]. Cui and co-workers reported a catalyst in which oxygen-coordinated tungsten single atoms are anchored on nickel sulfide nanosheets to regulate the interfacial water network. Combining experiment and theory, they showed that an atomic-scale W_1O motif induces a local interfacial electric field, markedly increasing the supply of free water in the inner Helmholtz plane (IHP) and reorienting interfacial water into an “H-down” configuration. This structural control promotes water activation and lowers the Volmer barrier from 2.41 to 1.02 eV, thereby accelerating the kinetics. The W_1O/NiS catalyst exhibits outstanding HER performance in 1 M KOH-overpotentials of 76 mV and 236 mV at 10 and 1000 mA cm^{-2}, respectively, and 98% retention of the initial activity after 300 h at 200 mA cm^{-2}-surpassing most reported Ni-based HER catalysts [60]. By targeting interfacial-water dynamics, the study clarifies how water activation governs the Volmer step. Extending this analysis, the engineered IHP environment reduces the enthalpic penalty for O-H bond cleavage and increases the population of weakly hydrogen-bonded molecules that serve as more labile proton donors, while the directed dipole orientation stabilizes the transition state through favorable field-dipole interactions. The single-atom W_1O sites

also reshape the local electronic structure at the metal-electrolyte boundary, modulating charge density on adjacent NiS atoms and tuning the interfacial potential drop, which together enhance electron transfer to adsorbed water and facilitate H* formation without over-strengthening H adsorption. As a result, both the apparent activation energy and the kinetic prefactor of the Volmer step improve, yielding high current densities at low overpotentials and durable operation under sustained alkaline conditions. More broadly, these findings underscore a general design paradigm for alkaline HER: concurrent optimization of intrinsic site energetics and the electric-double-layer microenvironment to control water orientation, solvation, and availability in the IHP, thereby directly addressing the mechanistic bottleneck that constrains overall reaction rates in alkaline media.

At the atomic level, Li and co-workers demonstrated that the kinetic barrier in the HER stems from the interfacial water structure rather than hydrogen adsorption energy. They showed that the electric double layer (EDL) controls the proton-transfer barrier and thus the kinetics of alkaline HER: the fundamental rate limitation is not a surface reaction per se, but cation-induced distortions of interfacial water in the EDL that impede transfer of protons from the bulk to the catalytic interface. Specifically, larger cations accumulate more strongly within the EDL, creating wider depletion gaps and a more discontinuous hydrogen-bond network, which disrupts proton-conduction pathways and severely suppresses the Grotthuss mechanism-thereby constituting the kinetic bottleneck in alkaline HER [61, 62].

Interfacial water structure-including molecular orientation, the hydrogen-bond network, and cation distributions within the double layer-is central to electrocatalysis [63]. Direct probing remains challenging because the interface is complex and

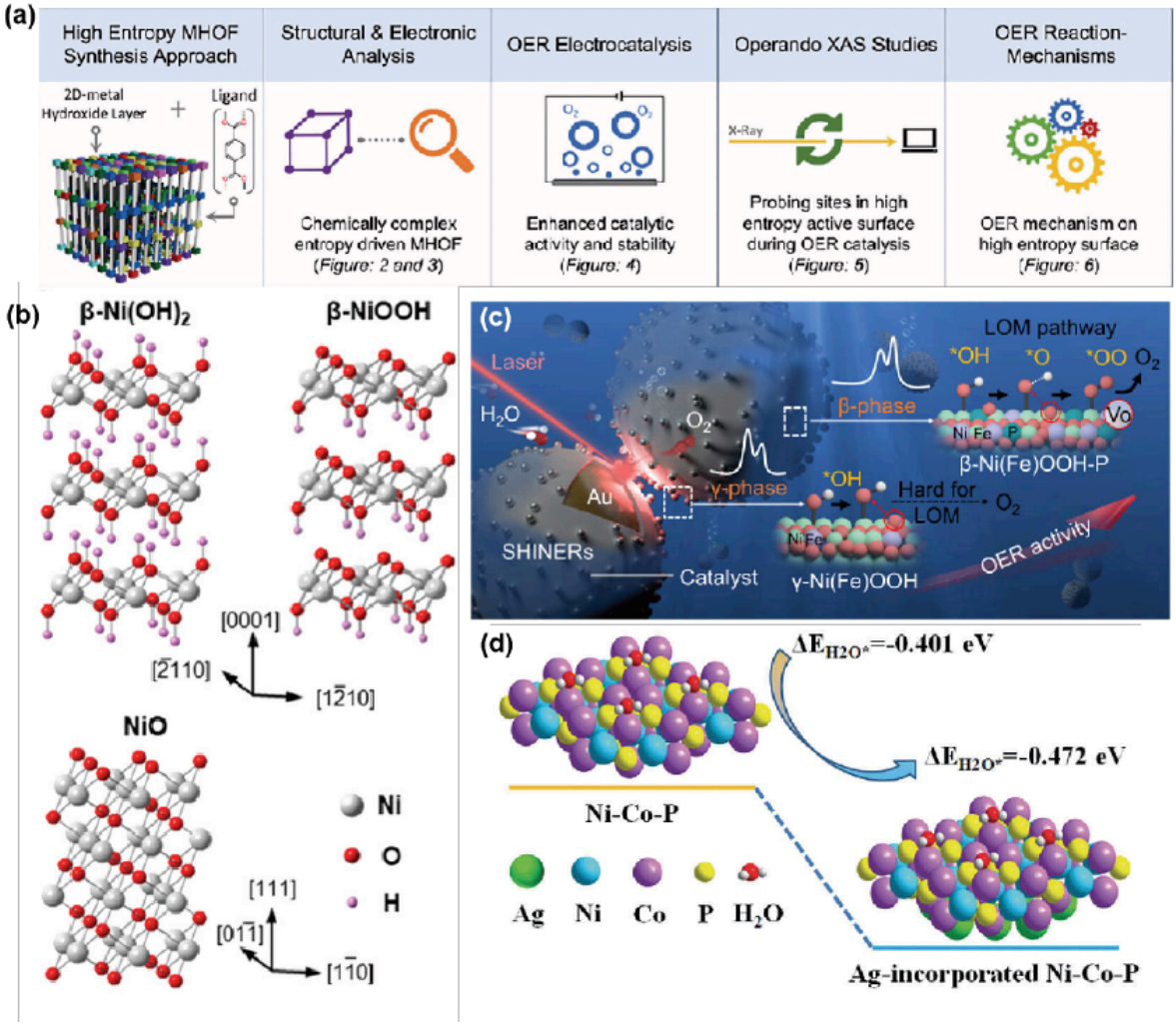

Figure 5: (**a**) Schematic illustration depicting the high-entropy metal hydroxide organic framework (HE-MHOF). Reprinted with permission.76 Copyright *2024 The Author(s).* (**b**) Atomic structure of *β*-Ni(OH)2, *β*-NiOOH, and NiO showing the similar hexagonal layered structure shared by them, which should favor the conversion between them. Reprinted with permission.77 Copyright *2024, American Chemical Society.* (**c**) Schematic of the OER mechanism of P-doped NiFe catalysts probed by in situ SHINERS. Reprinted with permission.78 Copyright *2025, American Chemical Society.* (**d**) water adsorption energies for the Ni–Co–P and Ag-incorporated Ni–Co–P. Reprinted with permission.75 Copyright Royal Society of Chemistry.

strongly perturbed by electrolyte ions. With advances *In-Raman* spectroscopy, however, dynamic changes in water structure can be monitored as a function of applied potential. Li and co-workers observed two potential-dependent transitions in molecular orientation and hydrogen-bond coordination number [64]. Inspired by water-management motifs in metalloenzymes, Yang and colleagues designed a biomimetic catalyst that bridges cobalt single atoms and ruthenium nanoclusters via a thio-oxo (S=O) linker: Co single atoms were introduced onto Ru nanoclusters and connected through S=O bridges (denoted Co_S-SO-Ru) to optimize the interfacial hydrogen-bond network. This architecture repels interfacial cations, promotes proton transfer, reduces the oxophilicity of Ru, and substantially enhances both HER activity and durability [65]. The approach provides a promising route to link interfacial-water structure with the alkaline-HER mechanism.

(2). Active-Site Optimization

Prior studies indicate that optimizing H* and OH* adsorption is essential for water activation and high efficiency in alkaline media; however, many catalysts that excel in acidic media underperform in base because sluggish water dissociation yields large overpotentials [66]. In mechanistic terms, achieving near-thermoneutral ΔG_{H^*} while maintaining suitably oxophilic sites for OH* stabilization lowers the barrier for the Volmer step and prevents kinetic throttling in the subsequent Heyrovsky/Tafel recombination. Accordingly, rational catalyst design targets coupled descriptors-hydroxyl binding energy, hydrogen adsorption free energy, and the activation enthalpy for interfacial H_2O cleavage-together with control of the electric double layer and interfacial water orientation, so as to increase the population of labile, weakly hydrogen-bonded water in the inner Helmholtz plane and enhance proton-coupled electron transfer. Hence, for alkaline HER catalysts it is crucial to tune H* and OH* binding-and, where possible, introduce dedicated water-dissociation sites-to accelerate the rate-limiting Volmer step. At the electrode level, complementary optimization of ionomer distribution, wettability, and hierarchical porosity maximizes accessible triple-phase boundaries, lowers charge-transfer resistance, and sustains high utilization at practical current densities, while durability considerations demand resistance to surface reconstruction, dissolution, and carbonate/impurity effects under dynamic operation.Platinum remains one of the most efficient HER catalysts in both acid and base and is widely employed owing to its combined activity and durability. However, its precious-metal cost constrains large-scale deployment [67]. As a result, low-cost alternatives based on 3d transition metals such as Ni and Co are attractive. In particular, transition-metal phosphides (TMPs)-*e.g.*, Ni_xP_y, Mo_xP_y, Co_xP_y, and Fe_xP_y-stand out for their chemical stability, high electrical conductivity, and noble-metal-like catalytic behavior [68]. From an electronic-structure perspective, mixed metallic/covalent M-P bonding affords high carrier density and tunable d-band states that can position ΔG_{H^*} near optimum values, while polarized M-P motifs furnish adjacent oxophilic and hydride-affinitive sites that facilitate bifunctional water activation and rapid H* formation. Under alkaline bias, robust TMP surfaces can maintain low charge-transfer resistance and favorable interfacial microenvironments, enabling reduced Volmer barriers without sacrificing corrosion resistance. Together, these characteristics outline a coherent pathway to precious-metal-lean HER electrodes that couple intrinsic activity with stability and manufacturability for AEMWE.

Among TMPs, NiCoP is a leading candidate for alkaline HER. Its high conductivity supports rapid electron transport, while bimetallic synergy promotes water adsorption and dissociation-the rate-determining step-thereby lowering the activation barrier and accelerating kinetics. Zhao and co-workers showed that heterostructures tailor the electronic states of active sites, tuning the hydrogen-adsorption free energy (ΔG_{H^*}) and the water-dissociation barrier, promoting reactant adsorption and intermediate formation/transfer, and expediting product desorption across the full pH range; in doing so, they established direct links between nanoscale structure and HER mechanism.

Layered transition-metal dichalcogenides (TMDs) such as MoS_2 are effective HER catalysts in acidic media but perform poorly in alkaline electrolytes because they lack OH^--adsorption sites [69]. To overcome this limitation, Pi and colleagues constructed a Mott-Schottky heterojunction catalyst, Mo_5N_6-MoS_2/HCNRs. The material was prepared by coating MoO_3 nanoribbons with polypyrrole (PPy), sulfurizing to obtain 2H-MoS_2/PPy, and pyrolyzing at 750°C under NH_3; During pyrolysis, PPy carbonized to hollow carbon nanoribbons (HCNRs), a fraction of MoS_2 nitrided to Mo_5N_6-MoS_2 nanosheets, and in-plane chemical bonding between the phases created the Mott-Schottky interface. This interface drives electron transfer from MoS_2 to metallic Mo_5N_6, activating otherwise inert MoS_2 basal planes. The catalyst delivers excellent HER performance in acidic, alkaline, and neutral media-overpotentials of 53-59 mV and Tafel slopes of 37.9-43.5 mV dec^{-1}-and exhibits remarkable durability; in overall water splitting, a two-electrode cell paired with NiFe-LDH requires only 1.49 V to achieve efficient H_2 production [70].

In summary, two broad approaches enhance water dissociation and accelerate reaction kinetics: (i) tuning adsorption characteristics and (ii) introducing new active sites through doping or by designing nanocomposite catalysts.

4. ELECTROCATALYSTS FOR THE ALKALINE OXYGEN EVOLUTION REACTION (OER)

In alkaline oxygen evolution, catalytic activity is constrained by two mechanistic bottlenecks: (i) scaling relations that couple the binding energies of *OH, *O, and *OOH in the classical adsorbate-evolution mechanism, and (ii) the accessibility of the lattice-oxygen mechanism (LOM), which depends on activating lattice oxygen and on the formation energy of oxygen vacancies. Highly active OER catalysts include IrO_2, RuO_2, and Ni/Co/Fe-based oxides and hydroxides (*e.g.*, NiFe-LDH) [71]. The use of earth-abundant transition-metal anodes (*e.g.*, Ni, Co, Fe) makes AEMWE attractive because its capital cost is lower than that of PEMWE. Nevertheless, the anodic OER in AEMWE generally requires substantial overpotential and displays sluggish kinetics.

At the anode, the OER oxidizes water or hydroxide to generate O_2, protons, and electrons via a complex four-electron pathway [72]. The adsorbate-evolution mechanism (AEM; not to be confused with "anion-exchange membrane") is widely accepted for alkaline OER and proceeds through the following elementary steps (M denotes an active site):

$$M + OH^- \rightarrow M\text{-}OH^* + e^- \quad (7)$$

$$M\text{-}OH^* + OH^- \rightarrow M\text{-}O^* + H_2O + e^- \quad (8)$$

$$M\text{-}O^* + OH^- \rightarrow M\text{-}OOH^* + e^- \quad (9)$$

$$M\text{-}OOH^* + OH^- \rightarrow M + O_2 + H_2O + e^- \quad (10)$$

Because these intermediates undergo repeated adsorption and desorption, the design of high-activity OER catalysts focuses on optimizing the binding and release of oxygenated species. Transition-metal-based materials-including oxides, sulfides, and phosphides-are intensively studied owing to their tunable *d*-electron structures, variable oxidation states, diverse architectures, and ability to modulate adsorption energies of O-containing intermediates [73]. Moreover, in both acidic and alkaline media, lattice-oxygen-involving surface reconstruction frequently occurs under OER conditions, complicating identification of the true active sites and mechanistic assignment [74]. Here we highlight two widely explored themes: surface reconstruction and the lattice-oxygen mechanism (LOM).

(1). Surface Reconstruction of OER Catalysts

The OER is a proton-coupled, four-electron process occurring at strongly oxidizing potentials, where newly formed oxy(hydroxide) species can alter surface composition and structure. Many non-oxide precatalysts reconstruct into oxide/oxyhydroxide layers during operation; for most systems, such reconstruction enhances activity. For example, under OER potentials NiCoP undergoes in situ oxidation to form a NiOOH/CoOOH-rich oxyhydroxide shell that acts as the true OER phase, while the NiCoP core provides electrical conductivity and mechanical support.

Using a template-guided strategy, Hu and co-workers prepared hierarchical Ni-Co-P hollow nanobricks (HNBs) with oriented nanosheet assemblies. Ag_2WO_4 nanocubes served as templates; deposition of Ni-Co precursors, thermal treatment, selective etching, and phosphidation yielded an open, hollow, ordered 2D-nanosheet architecture with high electrochemically active surface area, efficient electrolyte penetration, and facile gas release. As OER catalysts, Ni-Co-P HNBs required overpotentials of 270 mV (OER) and 107 mV (HER) to reach 10 mA cm^{-2}, and enabled overall water electrolysis at 10 mA cm^{-2} with only 1.62 V [75]. These results indicate that both spontaneous in situ oxidation and rationally engineered reconstruction can accelerate the OER on NiCoP-based systems.

Among perovskites, $Ba_{0.5}Sr_{0.5}Co_{0.8}Fe_{0.2}O_{3-\delta}$ (BSCF) ranks among the most active alkaline-OER catalysts. Time-resolved X-ray absorption spectroscopy captured dynamic self-reconstruction under OER conditions, and the newly formed metal oxy(hydroxide) species contribute substantially to the high alkaline-OER performance [76]. Similar surface reconstruction and metal leaching have been observed for layered oxides.

Surface reconstruction can also proceed without metal leaching. Spinel $NiCo_2O_4$-valued for its electrical conductivity and rich redox chemistry-is an excellent OER precatalyst that irreversibly transforms into NiOOH/CoOOH-rich oxyhydroxides, which constitute the true active phase. Beyond this generic picture, Yao and colleagues uncovered a facet-dependent reconstruction of β-$Ni(OH)_2$ under OER conditions. Combining ex situ and operando characterization, they showed that edge facets reconstruct into Ni-deficient, nanoporous $Ni_{1-X}O$ enriched in Ni_{3+}. *Operando* liquid-cell TEM and Raman spectroscopy further revealed the key role of β-NiOOH as a reaction intermediate en route to $Ni_{1-X}O$, defining a complete reconstruction pathway. This reconstruction markedly increases the exposure of active sites, accelerates Ni

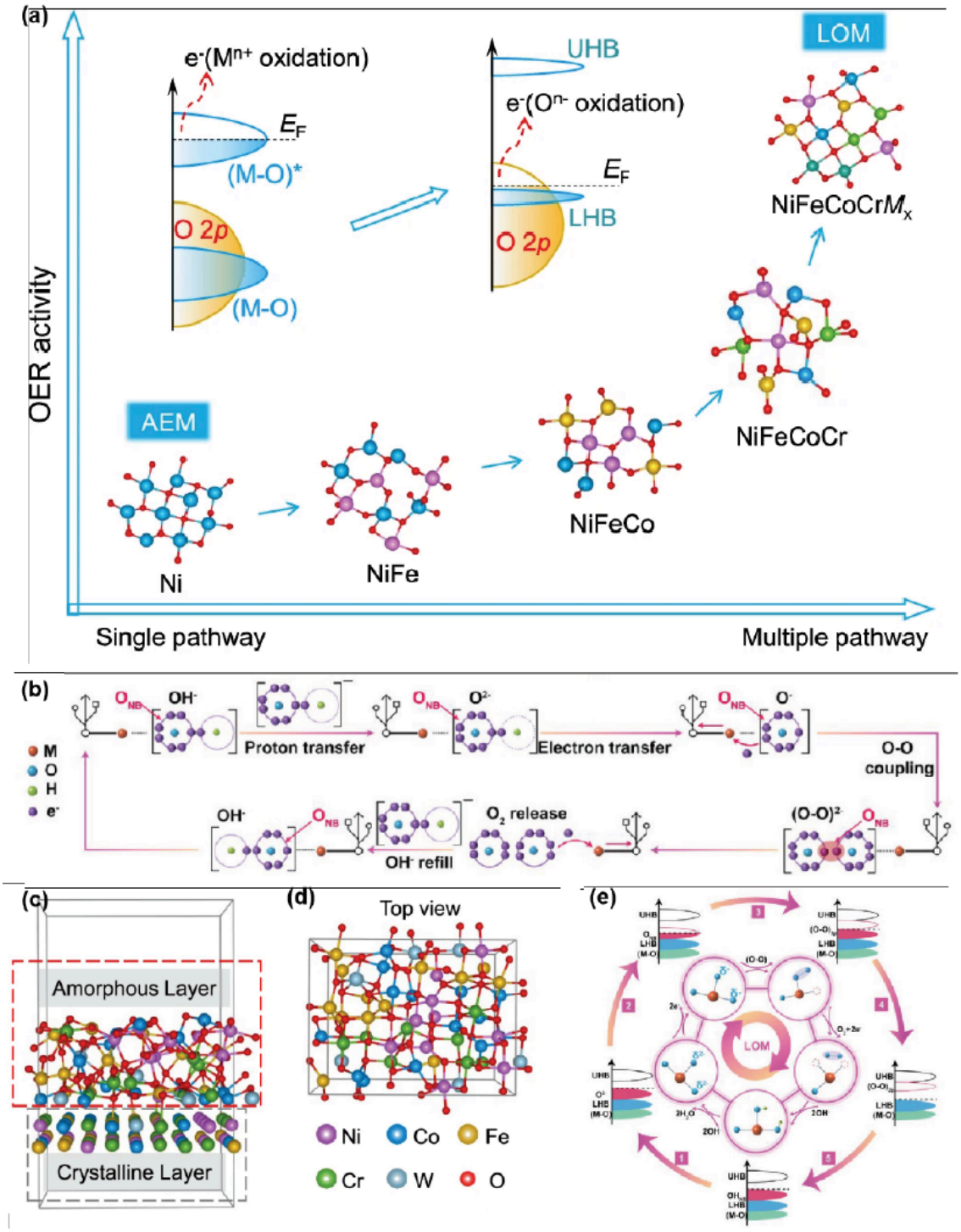

Figure 6: (**a**) Schematic of lattice oxygen activation. OER mechanism shifts from AEM to LOM by increasing the number of group elements. EF: Fermi level. Reprinted with permission.80 Copyright 2025, The Author(s). (**b**) Electron transfer pathways of LOM Reprinted with permission.79 Copyright 2022 Wiley-VCH. (**c, d**) Views of the NiFeCoCrW0.2 oxide model with top amorphous layers for DFT calculations. Reprinted with permission.80 Copyright 2025, The Author(s). (**e**) Electron-transfer process in conventional LOM route, where oxygen acts as the redox center. Reprinted with permission.79 Copyright 2022 Wiley-VCH.

oxidation kinetics, and optimizes the adsorption free energy of *OH, enhancing OER kinetics by 16-fold [77].

Distinct from typical reconstruction, NiFe-based catalysts often undergo phase segregation. Using *operando* quick-scan X-ray absorption spectroscopy (Q-XAFS), Han *et al.* correlated OER activity with dynamic changes in Fe coordination, whereas the Ni chemical state remained nearly constant. Low-coordination Fe centers-rather than Ni-serve as the dominant active sites in NiFeOOH. By applying reducing potential pulses, the authors selectively reduced Fe to induce low coordination and concomitant oxygen-vacancy formation. This pulse-driven dissolution-redeposition process maintains low-coordination Fe at the surface while Ni acts as a

structural scaffold, preventing irreversible Fe loss and preserving a highly active surface architecture [78]. These insights into the activity–stability relationship inform the design of efficient, durable OER catalysts.

(2). Lattice-Oxygen Mechanism (LOM)

Early descriptions of the OER largely followed the adsorbate-evolution mechanism. Subsequent studies of high-performance oxides and hydroxides showed that lattice oxygen can participate directly in O_2 formation-the lattice-oxygen mechanism (LOM)-which is especially relevant for oxides with suitable lattice structures [79]. A simplified sequence involves: (i) activation of lattice O; (ii) formation of oxygen vacancies (V$_O$) via heteroatom doping, lattice defects, or applied fields (a key step); and (iii) further oxidation of activated lattice O to *O or *OOH, which then couples with surface-adsorbed water or other intermediates to form O_2.

Xu and co-workers designed a high-entropy alloy, $NiFeCoCrW_{0.2}$, in which the high-entropy effect promotes multipath electron transfer and effectively activates the LOM pathway. *Operando* Raman spectroscopy, ^{18}O isotopic labeling, and differential electrochemical mass spectrometry (DEMS) verified lattice-oxygen participation and identified Ni-OO-Co dual sites as key LOM centers. Additional electrochemical tests in LOM-suppressing electrolytes (TMAOH, D_2O) further substantiated the dominance of the LOM pathway. The catalyst achieved excellent activity (η_{10} = 220 mV) and long-term stability (<5% potential drift over 90 days at 100 mA cm^{-2}) [80]. These findings broaden design principles for more efficient OER catalysts that operate via lattice-oxygen chemistry.

5. OPTIMIZATION OF AEMWE DEVICES

Anion-exchange membrane water electrolysis (AEMWE) enables efficient, low-cost conversion of renewable electricity into hydrogen and oxygen, providing a route to green H_2 production [81]. Effective optimization must proceed synergistically on three fronts: increasing catalyst activity, strengthening membrane-electrode interfacial stability, and refining mass-transport architecture [82].

Currently, AEMWE stacks typically rely on commercial catalysts, membranes, and electrodes. To further improve performance, future systems should adopt highly active, non-precious catalysts (*e.g.*, Ni$^-$, Fe$^-$, or Co$^-$based), pair them with anion-exchange

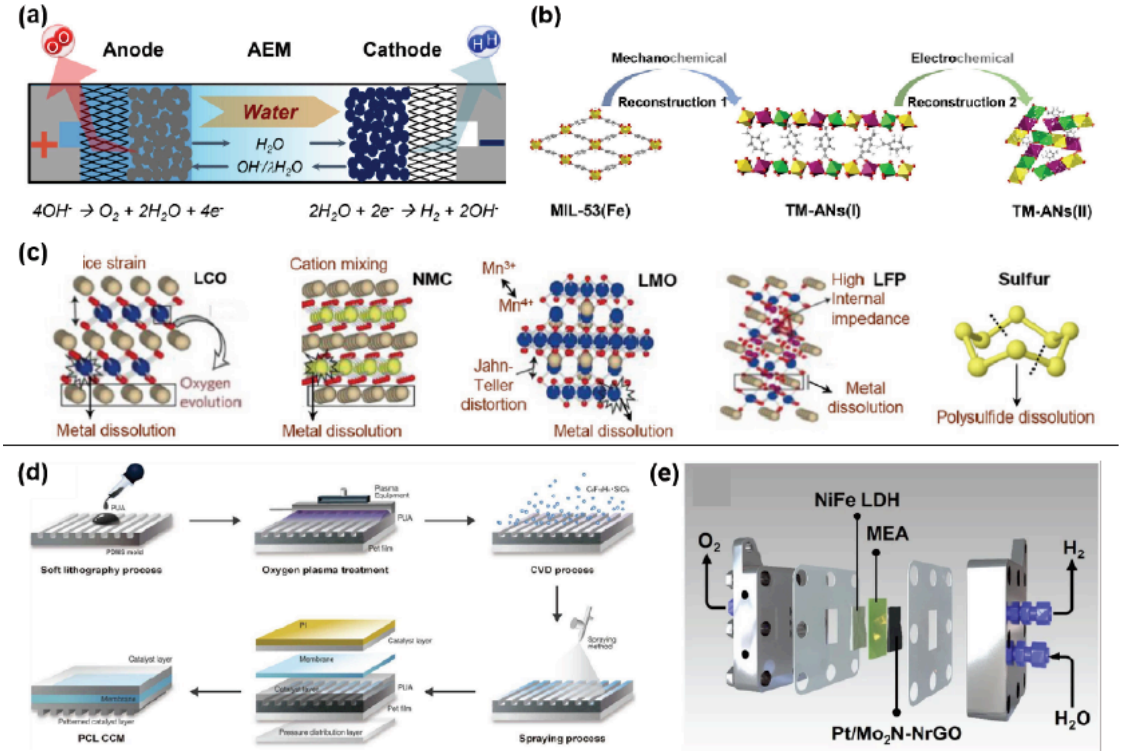

Figure 7: (**a**) Schematics showing hydroxide and water transport in an AEMWE cell. The electrolyte was 10 μM KOH and 100 mM of MgSO4 during in situ Raman measurement. Reprinted with permission.98 Copyright 2025 The Author(s). (**b**) Schematic for the structural evolution in the two-step reconstruction. Reprinted with permission.87 Copyright 2025 The Authors. (**c**) Schematics show aggravated instabilities at high temperatures for representative cathode materials. Reprinted with permission.85 Copyright 2025 Wiley-VCH. (**d**) Fabrication of decal transfer technique. Reprinted with permission.90 Copyright 2020 The Chemical Industry and Engineering Society of China, and Chemical Industry Press Co. (**e**) Schematic diagram of the AEMWE in 1.0 M KOH. .Reprinted with permission.82 Copyright 2025, The Author(s).

membranes that combine high OH^- conductivity with chemical robustness, and apply interfacial engineering to reinforce adhesion between the catalyst layers and the membrane [83-86]. For example, Li *et al.* designed an amorphous trimetallic electrocatalyst rich in organic ligands (TM-ANs(II)) to upgrade AEMWE performance. Prepared by mechanochemical and electrochemical reconstruction of a metal-organic framework, the catalyst retains terephthalate ligands that engage in *d-p* electronic interactions with the metal centers, promoting charge transfer and optimizing adsorption energies of oxygenated intermediates. As a result, oxygen-evolution reaction (OER) activity and durability are markedly enhanced; in an AEMWE cell at 55 °C, the device operated stably for >200 h at an industrially relevant current density of 500 mA cm^{-2} with a cell voltage of 1.69 V [87].

The membrane-electrode assembly (MEA)-comprising the AEM, an anode OER catalyst layer, and a cathode HER catalyst layer-is the core of an AEMWE device [88]. Two fabrication routes are widely used. In the catalyst-coated membrane (CCM) approach, catalyst inks are applied directly to both sides of the AEM and then hot-pressed with gas-diffusion layers (GDLs), effectively lowering interfacial resistance. In the catalyst-coated substrate (CCS) method, inks are first deposited on the GDLs to form electrodes, which are then hot-pressed with the membrane to assemble the MEA [89, 90]. Ito *et al.* identified an optimal configuration-CCM cathode and CCS anode-which guides tuning of catalyst loading and ionomer content for AEMWE [91].

The circulating electrolyte also plays a crucial role by governing ion transport and the catalyst-electrolyte interfacial area [92]. AEMWE commonly employs pure water, KOH, or K_2CO_3 [93]. With pure water, hydroxide transport depends solely on the membrane, so ohmic losses can be significant. By contrast, KOH or K_2CO_3 supplies additional OH^-, enhances membrane conductivity, and reduces resistive losses [94]. However, alkaline electrolytes can accelerate polymer degradation, undermining membrane stability and device lifetime [95]. To address this trade-off, Zhao *et al.* fabricated a composite AEM using a poly(ether ether ketone) (PEEK) base film and a low-$T_{(g)}$ quaternized polystyrene (QPS) resin. During hot pressing and operation, QPS transitions from a glassy to a rubbery state and acts as an “adhesive,” suppressing KOH-induced corrosion, strengthening the membrane-electrode interface, and facilitating rapid OH^- transport. The interfacial bonding strength reached 23.5 N mm^{-1}-two orders of magnitude higher than that of conventional high-$T_{(g)}$ (>200°C) poly(arylpiperidinium) membranes. The optimized interface improved OH^--transport kinetics, enabling pure-water electrolysis to deliver 1200 mA cm^{-2} at 1.8 V and 80 °C and continuous operation for 2464 h at 500 mA cm^{-2} [96].

Finally, tuning the operando states of the catalyst layers and the AEM is equally important [97]. Rito *et al.* showed that electrode architecture governs water back-diffusion and O_2 transport, which in turn shapes overpotential behavior. Electrodes with abundant active sites generate water near the AEM, establishing a steeper water-activity gradient that drives back-diffusion, improves membrane hydration and mass transport, and lowers losses. By adjusting ink additives, their AEMWE cell sustained 2 A cm^{-2} for >1000 h [98, 99]. In short, beyond membranes and anode/cathode catalysts, optimizing binders, GDLs, and other balance-of-cell components is essential for high-performance AEMWE [100]. The electrolyte operating conditions and catalyst preparation strategies significantly influence the performance of AEM water electrolysis (AEMWE) systems (Table **1**). The key factors involve optimizing the electrolyte's ionic conductivity and the catalyst's catalytic efficiency, as well as improving membrane-electrode assembly (MEA) design. The electrolyte composition and temperature directly affect the electrolysis performance. For instance, a high ionic conductivity is crucial for reducing ohmic resistance and enhancing charge transfer. Electrolytes with a concentration of 1 M KOH and temperatures around 60-90°C are commonly used, as they provide a balance between ionic conductivity and electrochemical reaction rates. However, maintaining high ionic conductivity in diluted electrolytes or pure water can be challenging. This is because lower concentrations reduce the concentration of OH^- ions, limiting the reaction kinetics. MEA fabrication methods also play a crucial role in optimizing electrolysis performance. The ionomer-free gapless catalyst-bridging method (GCB) for MEA fabrication offers advantages by ensuring better interfacial contact between the catalyst layer (CL), anion exchange membrane (AEM), and gas diffusion layer (GDL). This design minimizes contact resistance, enhances mass transfer, and ensures more effective use of active sites. This approach contrasts with conventional methods like CCM and CCS, where the ionomer binder can block active sites and increase resistance. The trade-offs in catalyst preparation include balancing activity with stability. For example, Fe-modulated Raney-Ni electrodes, while effective in improving both hydrogen and oxygen evolution reaction kinetics, can face challenges such as lower conductivity in their oxide form. On the other hand, high-entropy catalysts or layered metal hydroxides offer better stability but may require more intricate fabrication methods. Achieving the optimal structure,

which enhances the intrinsic activity and ensures durability under industrial operating conditions, remains a key focus. In summary, improving AEMWE performance involves optimizing both the electrolyte composition and catalyst structure. The integration of efficient catalysts with a well-designed MEA, like the GCB method, can significantly reduce resistance, increase active site utilization, and ensure long-term stability, addressing both the electrochemical performance and the mechanical durability of the system [19, 101, 109].

CONCLUSIONS AND OUTLOOK

This review examines recent advances in AEMWE, with particular emphasis on innovations that enhance membrane conductivity, elucidate degradation mechanisms, and guide electrocatalyst design. AEMWE has emerged as a strong contender for green-hydrogen production owing to its high energy efficiency, reliance on non-precious-metal catalysts, and favorable cost profile. Compared with conventional AWE, AEMWE employs high-performance anion-exchange membranes that improve ionic selectivity, thereby suppressing gas crossover and increasing hydrogen purity as well as overall energy efficiency. In addition, its capability to operate at high current densities with rapid dynamic response better accommodates the intermittency of wind and solar resources. Nevertheless, long-term stability and reliability at high current remain key limitations, particularly with respect to membrane durability and catalyst stability. Accordingly, the development of high-performance, low-cost membranes and catalysts remains a central research priority.

Further Optimization and Durability Improvement of Membrane Materials:

AEMs currently face degradation issues in highly alkaline environments, which not only affect their conductivity but may also lead to a reduction in mechanical strength and structural stability, ultimately compromising the long-term stability of the device. Therefore, future research should prioritize the design of more durable membranes with enhanced conductivity. Specifically, researchers can improve the chemical and thermal stability of membranes by modifying their molecular structure, optimizing crosslinking, and incorporating reinforcing materials such as inorganic fillers. Additionally, optimizing water management technology is critical for improving membrane durability. For example, enhancing the membrane's hydration management capability can ensure its stability under varying temperature and humidity conditions, minimizing performance degradation due to membrane expansion and contraction. These strategies will enable AEMs to operate stably at higher current densities and voltages, meeting the requirements for large-scale hydrogen production.

Table 1: The Relationship between Electrolyte Operation, Catalyst Preparation in the MEA, and AEMWE Performance

Catalysts (OER)	η@10 $mAcm^{-2}$ (V)	Catalysts (HER)	η@10 $mAcm^{-2}$ (V)	Electrolyze	AEM	Ref.
NiFeSe	0.19 V (vs. RHE)	-	-	1 M KOH	8800 mA cm^{-2} @ 2.0 V	Angew. Chem. 2025, e202517132 [101]
-	-	$PtNiO_xH_2/C$	0.0396 V (vs. RHE)	1 M KOH	2 A cm^{-2} @ 1.90 V	Angew. Chem. Int. Ed. 2025, 64, e202422062 [102]
$CoCrO_x$	-	-	-	1 M KOH	1.5 A cm^{-2}@ 2.1 V	Nature Communications, 2024, 15, 3416 [103]
-	-	Pt-HEA-cluster/CeO_2/C	0.027 V(vs. RHE)	1.0 M KOH	2 A cm^{-2} @ 1.74 V120 h stability @ 500 mA cm^{-2}	Adv. Mater. 2025, e2514269 [104]
NFA-CA	0.169 V (vs. RHE)	NFA-CA	0.027 V (vs. RHE)	1 M KOH	1 A cm^{-2} @ 1.56 V	Adv. Energy Mater. 2025, 15, 2501634 [106]
NiFeCoLi/NF	-	-	-	1 M KOH	2000 m A cm^{-2}@ 1.90 V	Adv. Energy Mater. 2025, e04707 [106]
-	-	FeP-Ni_5P_4-CoP/PBA	0.099 V (vs. RHE)	1 M KOH	500 m A cm^{-2}@ 2.20 V	J. Colloid Interface Sci. 2026, 703, 139276. [107]
FeZnNNiCoV	0.220 V (vs. RHE)	-	-	1 M KOH	1 A cm^{-2} @ 1.76 V	Adv. Mater. 2025, 37, 2509042. [108]
Ru-NCO/rGO	0.219 V (vs. RHE)	-	-	1.0 M KOH	1.0 A cm^{-2}@ 1.89 V	Adv. Energy Mater. 2025, 15, e01952. [19]
NiFe	-	-	-	1 M KOH	1 A cm^{-2} @ 1.55 V2 A cm^{-2} @ 1.70 V	Adv. Mater. 2025, e09805 [109]

Development and Optimization of Non-Precious Metal Catalysts:

Although precious metal catalysts, such as platinum and iridium, are crucial for water electrolysis due to their excellent catalytic performance, their high cost hinders the commercialization of AEMWE technology. Future research will increasingly focus on the development and optimization of non-precious metal catalysts, particularly transition metals such as nickel, cobalt, and iron, along with their alloy catalysts. Non-precious metal catalysts typically offer lower costs and satisfactory catalytic performance, but their stability and efficiency remain key challenges for technological advancement. By adjusting the nanostructure, electronic structure, and surface defects of the catalyst, catalytic active sites can be optimized, thereby enhancing catalytic efficiency. For instance, synthesizing cobalt-nickel alloy catalysts with high surface activity and stability, or developing transition metal phosphide catalysts with tunable electronic structures, can significantly reduce the overpotential of the hydrolysis reaction and improve hydrogen production efficiency. Moreover, catalyst stability and durability remain crucial research areas, with efforts focused on material design to suppress catalyst corrosion and precipitation, ensuring their reliable operation at high current densities over extended periods.

Structure and System Optimization of Electrolyzer Devices:

The design of the AEMWE device structure is pivotal in determining its energy efficiency and cost-effectiveness. Future research should focus on optimizing electrode design, membrane-electrode assembly (MEA) structure, and flow field design. First, electrode design should ensure the uniform distribution of the catalyst layer and efficient utilization of catalytic active sites. By enhancing the interfacial adhesion between the electrode and the membrane and reducing interfacial resistance, overall efficiency can be improved. Specifically, optimizing the interface between the membrane and electrode using adhesives with good mechanical strength can reduce interfacial resistance, improve membrane conductivity, and enhance catalytic efficiency. Second, the flow field design is equally important. An optimized flow field structure can improve the flow of reactant gases and electrolytes, reduce gas crossover, and enhance hydrogen-oxygen separation, while also optimizing electrolyte transport paths to reduce ohmic losses and improve system efficiency. Additionally, zero-gap design is an effective strategy to improve AEMWE performance, as it minimizes the electrolyte conduction path and significantly reduces internal resistance.

Adaptability to Renewable Energy and Dynamic Load Response:

As AEMWE is typically coupled with renewable energy sources like solar and wind power, the variability of these energy sources imposes higher demands on the stability of hydrogen production systems. Future research should focus on advancing AEMWE systems to better adapt to and respond to fluctuations in renewable energy supply. Specifically, these systems must be capable of quickly adjusting their load to maintain stable hydrogen production despite intermittent electricity supply. To achieve this, AEMWE system design should emphasize dynamic responsiveness. For example, by optimizing membrane materials and catalysts, the system should be capable of switching flexibly between low and high loads while maintaining high energy conversion efficiency. Furthermore, enhancing the system's ability to withstand load fluctuations and minimizing equipment loss due to power supply variations will be crucial for future AEMWE optimization. This will ensure that the system can operate stably, especially in environments with large-scale renewable energy integration.

System Integration and Synergy with Multiple Energy Sources:

AEMWE technology should not be confined to standalone operation but rather integrated with other energy systems to enhance overall energy utilization efficiency. Future research should aim to integrate AEMWE with other renewable energy technologies such as solar photovoltaics, wind power, and energy storage systems, optimizing the management and distribution of energy flows. For example, in large-scale renewable energy scenarios, AEMWE could be coupled with energy storage systems to convert surplus renewable energy into hydrogen and store it to address energy demand fluctuations. In such a synergistic system, AEMWE not only mitigates the intermittency of renewable energy but also enhances overall system efficiency and economic viability. Furthermore, future AEMWE systems could optimize energy flow distribution via intelligent control systems, dynamically matching hydrogen production to electricity demand, thereby achieving optimal energy allocation and maximizing energy utilization.

Large-Scale Commercialization and Economic Analysis:

While AEMWE has demonstrated significant performance in laboratory settings, challenges remain in terms of equipment costs, operational costs, and technological feasibility for large-scale commercialization. Future research will focus on the

economic analysis of systems and devices to enable the low-cost production of materials and components. Specifically, developing low-cost, high-performance electrolyzer membranes and catalysts is crucial to reducing the overall cost of AEMWE systems. In addition to material cost efficiency, optimizing manufacturing processes will also play an important role in cost reduction. For instance, improving membrane production efficiency, optimizing catalyst synthesis methods, and designing modular systems can significantly reduce manufacturing costs. Moreover, to accelerate AEMWE's commercialization, it is vital to strengthen policy support and market guidance to promote the large-scale application of hydrogen production technologies, ensuring that AEMWE plays a pivotal role in the global energy transition.

CREDIT AUTHORSHIP CONTRIBUTION STATEMENT

Y. S. - Conceptualization, Literature curation, Writing-original draft, Writing-review & editing.

Z. Z. - Data curation, Visualization, Writing-support.

Z. W. - Literature search, Validation, Writing-support.

Y. G. - Formal analysis, Writing-review.

H. L. - Supervision, Writing-review & editing.

D. Z. - Supervision, Writing-review & editing.

X. W. - Conceptualization, Supervision, Writing-review & editing.

All the authors discussed the content and commented on the manuscript.

DECLARATION OF COMPETING INTEREST

The authors declare that they have no known competing financial interests or personal relationships that could have appeared to influence the work reported in this paper.

ACKNOWLEDGMENT

The authors sincerely appreciate the academic platform and resources provided by their research group/department, and are grateful to colleagues for their valuable suggestions during discussions.

REFERENCES

[1] Sun, F.;Tang, Q.; Jiang, D.-e. Theoretical Advances in Understanding and Designing the Active Sites for Hydrogen Evolution Reaction. ACS Catal. 2022, 12, 8404-8433. https://doi.org/10.1021/acscatal.2c02081

[2] Zhao, S.;Li, Z. X.;Guo, H. T.;Li, J.;Liu, Z. L.;Wang, P. F.;Wang, L. L.; Yi, T. F. Critical Role of Carbon Substrates in Optimizing Ru-Based HER Catalysts: From Dimensional Insights to Metal-Support Interactions Engineering. Adv. Funct. Mater. 2025, 25, e09799. https://doi.org/10.1002/adfm.202509799

[3] Jia, Y.;Zhang, Y.;Xu, H.;Li, J.;Gao, M.; Yang, X. Recent Advances in Doping Strategies to Improve Electrocatalytic Hydrogen Evolution Performance of Molybdenum Disulfide. ACS Catal. 2024, 14, 4601-4637. https://doi.org/10.1021/acscatal.3c05053

[4] Lang, C.;Xu, Y.; Yao, X. Perfecting HER catalysts via defects: Recent advances and perspectives. Chin. J. Catal. 2024, 64, 4-31. https://doi.org/10.1016/S1872-2067(24)60105-1

[5] Li, J.;Li, L.;Wang, J.;Cabot, A.; Zhu, Y. Boosting Hydrogen Evolution by Methanol Oxidation Reaction on Ni-Based Electrocatalysts: From Fundamental Electrochemistry to Perspectives. ACS Energy Lett. 2024, 9, 853-879. https://doi.org/10.1021/acsenergylett.3c02678

[6] Henkensmeier, D.;Cho, W.-C.;Jannasch, P.;Stojadinovic, J.;Li, Q.;Aili, D.; Jensen, J. O. Separators and Membranes for Advanced Alkaline Water Electrolysis. Chem. Rev. 2024, 124, 6393-6443. https://doi.org/10.1021/acs.chemrev.3c00694

[7] Wang, Y.;Yan, H.; Fu, H. Recent advances and modulation tactics in Ru- and Ir-based electrocatalysts for PEMWE anodes at large current densities. eScience 2025, 5, 100323. https://doi.org/10.1016/j.esci.2024.100323

[8] Feng, P.;Yang, K.;Liu, X.;Zhang, J.; Li, Z.-P. A review of advanced SOFCs and SOECs: materials, innovative synthesis, functional mechanisms, and system integration. eScience 2025, 5, 100460. https://doi.org/10.1016/j.esci.2025.100460

[9] Lu, Z.;Niu, W.;He, Y.;Jin, L.;Li, W.;Yang, X.;Sun, K.;Yan, Q.;Chen, J.;Zhang, J.;Shi, W.;Wei, C.;Li, Y.;Lu, H.; Zhang, B. Molybdate-Leaching-Induced Bimetallic Catalyst for Efficient Anion Exchange Membrane Water Electrolysis. Adv. Funct. Mater. 2025, 17, 2505626. https://doi.org/10.1002/adfm.202505626

[10] Son, Y. J.;Mirshekari, G.;Raaijman, S. J.; Corbett, P. J. Technology Landscape of Anion Exchange Membrane Water Electrolyzers: Where Are We Today? ACS Energy Lett. 2025, 10, 3058-3063. https://doi.org/10.1021/acsenergylett.5c01366

[11] Ma, W.;Morales-Vidal, J.;Tian, J.;Liu, M.-T.;Jin, S.;Ren, W.;Taubmann, J.;Chatzichristodoulou, C.;Luterbacher, J.;Chen, H. M.;López, N.; Hu, X. Encapsulated Co–Ni alloy boosts high-temperature CO2 electroreduction. Nature 2025, 641, 1156-1161. https://doi.org/10.1038/s41586-025-08978-0

[12] Chen, J.;Ma, Y.;Cheng, C.;Huang, T.;Luo, R.;Xu, J.;Wang, X.;Jiang, T.;Liu, H.;Liu, S.;Huang, T.;Zhang, L.; Chen, W. Cobalt-Doped Ru@RuO2 Core–Shell Heterostructure for Efficient Acidic Water Oxidation in Low-Ru-Loading Proton Exchange Membrane Water Electrolyzers. J. Am. Chem. Soc. 2025, 147, 8720-8731. https://doi.org/10.1021/jacs.4c18238

[13] Li, S.;Deng, L.;Hung, S. F.;Zhao, S.;Wang, L.;Hao, Y.;Long, Y.;Li, B.;Hsu, Y. H.;Chen, Y. Y.;Zhang, Y.;Chen, T. Y.;Hu, F.;Li, L.;Hu, Y.;Wu, Y.; Peng, S. Embedded Ir-Ru Single-Atom Alloy with Self-Limiting Motifs for Sustainable Proton Exchange Membrane Water Electrolysis. Adv. Mater. 2025, 17, e07340.

[14] Dai, M.;Zhao, D.; Wu, X. Research progress on transition metal oxide based electrode materials for asymmetric hybrid capacitors. Chin. Chem. Lett. 2020, 31, 2177-2188. https://doi.org/10.1016/j.cclet.2020.02.017

[15] Zhang, Q.;Hao, Y.;Chen, H.;Li, J.;Zeng, Y.;Xiong, J.;Cheng, Y.;Tricoli, A.; Li, F. Toward Energy-Efficient Alkaline Water Electrolysis: Advances in Mass Transport Optimization and Electrolyzer Design. Adv. Energy Mater. 2025, 14, e04039. https://doi.org/10.1002/aenm.202504039

[16] Zou, W.;Tang, G.;Peng, K.;Mo, X.;Hu, T.;Yang, Z.; Xu, T. Quinuclidinium-Based Microporous Anion Exchange Membranes for Water Electrolysis. Angew. Chem. Int. Ed. 2025, 7, e202514264. https://doi.org/10.1002/anie.202514264

[17] Yuan, Z.;Liu, Y.;Li, H.;Kong, Q.;Sun, H.;Qiao, Q.;Zhang, X.;Liu, H.;Tan, Y.;Ge, Q.;Xu, T.;Dai, X.; Zhang, X. Poly(terphenyl-diphenylmethane piperidinium) anion

exchange membranes assemble with non-precious metal electrodes for high-performance water electrolysis. Sci. China Mater. 2025. https://doi.org/10.1007/s40843-025-3631-1

[18] Klingenhof, M.;Trzesniowski, H.;Koch, S.;Zhu, J.;Zeng, Z.;Metzler, L.;Klinger, A.;Elshamy, M.;Lehmann, F.;Buchheister, P. W.;Weisser, A.;Schmid, G.;Vierrath, S.;Dionigi, F.; Strasser, P. High-performance anion-exchange membrane water electrolysers using NiX (X = Fe,Co,Mn) catalyst-coated membranes with redox-active Ni–O ligands. Nat. Catal. 2024, 7, 1213-1222. https://doi.org/10.1038/s41929-024-01238-w

[19] Tian, C.;Liu, R.;Lv, Z.;Wang, C.;Liu, W.;Dong, F.;Feng, X.;Yang, W.; Wang, B. Heterogeneous Support Effects for Enhanced Performance in Anion Exchange Membrane Water Electrolysis. Adv. Energy Mater. 2025, 15, e01952. https://doi.org/10.1002/aenm.202501952

[20] Li, H.;Lin, Y.;Duan, J.;Wen, Q.;Liu, Y.; Zhai, T. Stability of electrocatalytic OER: from principle to application. Chem. Soc. Rev. 2024, 53, 10709-10740. https://doi.org/10.1039/D3CS00010A

[21] Zhang, L.;Qi, F.;Ren, R.;Gu, Y.;Gao, J.;Liang, Y.;Wang, Y.;Zhu, H.;Kong, X.;Zhang, Q.;Zhang, J.; Wu, L. Recent Advances in Green Hydrogen Production by Electrolyzing Water with Anion-Exchange Membrane. Research 2025, 8, 0677. https://doi.org/10.34133/research.0677

[22] Liu, Y.;Vijayakumar, P.;Liu, Q.;Sakthivel, T.;Chen, F.; Dai, Z. Shining Light on Anion-Mixed Nanocatalysts for Efficient Water Electrolysis: Fundamentals, Progress, and Perspectives. Nano-Micro Lett. 2022, 14, 43. https://doi.org/10.1007/s40820-021-00785-2

[23] Chen, Z.;Yang, M.;Li, Y.;Gong, W.;Wang, J.;Liu, T.;Zhang, C.;Hou, S.;Yang, G.;Li, H.;Jin, Y.;Zhang, C.;Tian, Z.;Meng, F.; Cui, Y. Termination-acidity tailoring of molybdenum carbides for alkaline hydrogen evolution reaction. Nat. Commun. 2025, 16, 418. https://doi.org/10.1038/s41467-025-55854-6

[24] Wang, L.-L.;Wang, X.-R.;Wang, H.-J.;Zhang, C.;Li, J.-J.;Feng, G.-J.;Cheng, X.-X.;Qin, X.-R.;Yu, Z.-Y.; Lu, T.-B. Tailoring Lewis Acidity of Metal Oxides on Nickel to Boost Electrocatalytic Hydrogen Evolution in Neutral Electrolyte. J. Am. Chem. Soc. 2025, 147, 7555-7563. https://doi.org/10.1021/jacs.4c16596

[25] Chen, Y.;Tang, Z.;Liu, Z.;Huang, W. H.;Yeh, M. H.;Pao, C. W.;Tao, H.;Xu, M.;Dong, Z.;Yuan, L.;Pu, M.;Li, B.;Yang, G.;Guo, Y.;Hu, Z.; Zhu, Y. Toward the Ideal Alkaline Hydrogen Evolution Electrocatalyst: a Noble Metal-Free Antiperovskite Optimized with A-Site Tuning. Adv. Mater. 2025, 37, 2504607. https://doi.org/10.1002/adma.202504607

[26] Xu, S.;Feng, S.;Yu, Y.;Xue, D.;Liu, M.;Wang, C.;Zhao, K.;Xu, B.; Zhang, J.-N. Dual-site segmentally synergistic catalysis mechanism: boosting CoFeSx nanocluster for sustainable water oxidation. Nat. Commun. 2024, 15, 1720. https://doi.org/10.1038/s41467-024-45700-6

[27] Chen, M.;Kitiphatpiboon, N.;Feng, C.;Abudula, A.;Ma, Y.; Guan, G. Recent progress in transition-metal-oxide-based electrocatalysts for the oxygen evolution reaction in natural seawater splitting: A critical review. eScience 2023, 3, 100111. https://doi.org/10.1016/j.esci.2023.100111

[28] Yue, K.;Lu, R.;Gao, M.;Song, F.; Dai, Y. Polyoxometalated metal-organic framework superstructure for stable water oxidation. Science 2025, 388, 430-436. https://doi.org/10.1126/science.ads1466

[29] Zheng, Y.;Serban, A.;Zhang, H.;Chen, N.;Song, F.; Hu, X. Anion Exchange Ionomers Enable Sustained Pure-Water Electrolysis Using Platinum-Group-Metal-Free Electrocatalysts. ACS Energy Lett. 2023, 8, 5018-5024. https://doi.org/10.1021/acsenergylett.3c01866

[30] Akay, Ö.;Monfort-Castillo, M.;St Francis, T.;Becker, J.;Saravanabavan, S.;Romero-Calvo, Á.; Brinkert, K. Magnetically induced convection enhances water electrolysis in microgravity. Nat. Chem. 2025. https://doi.org/10.1038/s41557-025-01890-0

[31] Xiong, H.;Zhuang, R.;Cheng, B.;Liu, D.;Du, Y.;Wang, H.;Liu, Y.;Xu, F.; Wang, H. Self-Supported Metallic Alkaline Hydrogen Evolution Electrocatalysts Tolerant for Ampere-Level Current Densities. Adv. Energy Mater. 2024, 15, 2404077. https://doi.org/10.1002/aenm.202404077

[32] Liu, X.;Chi, J.;Zhao, Y.;Huang, R.;Zhang, H.;Fu, J.;Ren, Z.;Han, Y.;Wei, T.;Song, W.;Yu, H.; Shao, Z. Achieving 2400+ Hours Pure Water-Fed Electrolysis via Hydroxide Exchange Membrane-Electrodes Interface Engineering. Adv. Energy Mater. 2025. https://doi.org/10.1002/aenm.202503388

[33] Song, W.;Ge, X.;Wu, L.;Yang, Z.; Xu, T. Bottlenecks of commercializing anion exchange membranes for energy devices. Joule 2025, 9, 102051. https://doi.org/10.1016/j.joule.2025.102051

[34] Miao, R. K.;Fan, M.;Wang, N.;Zhao, Y.;Li, F.;Liu, M.;Arabyarmohammadi, F.;Liang, Y.;Ni, W.;Xie, K.;Chen, Y.;Sun, P.;Huang, J. E.;Wu, J.;Kim, J.;O'Brien, C. P.;Xiao, Y. C.;Guo, Z.;Papangelakis, P.;Shayesteh Zeraati, A.;Xu, Y.;Dinh, C.-T.;Sargent, E. H.; Sinton, D. CO electrolysers with 51% energy efficiency towards C2+ using porous separators. Nat. Energy 2025. https://doi.org/10.1038/s41560-025-01846-1

[35] Zhao, D.;Liu, X.;Zhang, W. c.;Wu, X.; Cho, Y. R. Highly Efficient and Stable Mo-CoP3@FeOOH Electrocatalysts for Alkaline Seawater Splitting. Small Methods 2023, 8, 2301474. https://doi.org/10.1002/smtd.202301474

[36] Nie, Y.;Fan, L.;Mao, J.;Pan, J.;Hu, C.;Zhu, A.;Hong, Y.;Xie, Z.; Zhang, Q. Effects of cationic groups on poly(biphenyl alkylene)-based anion-exchange membranes for water electrolyzer. J. Membr. Sci. 2025, 735, 124556. https://doi.org/10.1016/j.memsci.2025.124556

[37] Jin, W.;Kim, E. H.;Lee, S.;Yu, S.;Han, H.;Kim, G.;Lee, S. W.;Jang, J.;Lee, C. E.;Shim, W.; Park, C. Tandem Interactive Sensing Display De-Convoluting Dynamic Pressure and Temperature. Adv. Funct. Mater. 2021, 31, 2010492. https://doi.org/10.1002/adfm.202010492

[38] Zhang, H.;He, X.;Feng, H.;Li, C.; Li, M. A poly(binaphthyl-co-terphenyl quinuclidinium) anion exchange membrane with excellent alkaline stability and anion conductivity. J. Mater. Chem. A 2024, 12, 23570-23576. https://doi.org/10.1039/D4TA03241A

[39] Li, J.;Li, W.;Wang, X.;Pan, D.;Sa, R.;Xiao, M.;Liu, C.;Xing, W.; Zhu, J. A microphase separation anion exchange membrane based on poly(terphenyl piperidinium)/cationic polyelectrolyte for high-performance AEMWEs. J. Membr. Sci. 2025, 730, 124206. https://doi.org/10.1016/j.memsci.2025.124206

[40] Ma, L.; Wang, T. Rational Understanding Hydroxide Diffusion Mechanism in Anion Exchange Membranes during Electrochemical Processes with RDAnalyzer. Angew. Chem. Int. Ed. 2024, 63, e202403614. https://doi.org/10.1002/anie.202403614

[41] Wu, D.;Zhang, N.;Gao, W.;Li, Q.;Gao, X.;Wang, S.; Che, Q. Novel anion-exchange membranes with accelerated hydroxide ion conduction through a quaternized covalent organic framework-doped electrospinning binary polymer. J. Mater. Chem. A 2024, 12, 28805-28817. https://doi.org/10.1039/D4TA04614E

[42] Liu, W.;Geng, Z.;Guo, S.;Liu, L.;Zhao, L.;Qu, C.;Xia, Q.;Cai, H.;Zhao, X.;Zhu, J.;Chen, J.;Jin, L.; Zhang, C. Hydrogen-Bonding Enhanced Anion Exchange Membrane for High Performance Alkaline Water Electrolysis. Adv. Energy Mater. 2025, 1, e03110. https://doi.org/10.1002/aenm.202503110

[43] Wang, C.;Wang, T.;Chen, D.;Ling, Q.;Liu, C.;Li, X.;Wei, H.; Ding, Y. Insights into the Alkaline Stability of Poly(arylene piperidinium)s. Macromolecules 2025, 58, 8335-8343. https://doi.org/10.1021/acs.macromol.5c01603

[44] Liu, H.;Zhao, D.;Dai, M.;Zhu, X.;Qu, F.;Umar, A.; Wu, X. PEDOT decorated CoNi2S4 nanosheets electrode as bifunctional electrocatalyst for enhanced electrocatalysis.

Chem. Eng. J. 2022, 428, 131183.
https://doi.org/10.1016/j.cej.2021.131183

[45] Nguyen, T. D.;Yeo, D.;Chitumalla, R. K.;Kim, S. J.;Jeong, G. H.;Kwun, D. G.;Jang, J.;Jung, I. H.; Seo, J. Y. Tailor-Made Buffer Materials: Advancing Uniformity and Stability in Perovskite Solar Cells. Adv. Energy Mater. 2024, 15, 2403633.
https://doi.org/10.1002/aenm.202403633

[46] Pan, D.;Chen, S.; Jannasch, P. Alkali-Stable Anion Exchange Membranes Based on Poly(xanthene). ACS Macro Lett. 2022, 12, 20-25.
https://doi.org/10.1021/acsmacrolett.2c00672

[47] Willdorf-Cohen, S.;Zhegur-Khais, A.;Ponce-González, J.;Bsoul-Haj, S.;Varcoe, J. R.;Diesendruck, C. E.; Dekel, D. R. Alkaline Stability of Anion-Exchange Membranes. ACS Appl. Energy Mater. 2023, 6, 1085-1092.
https://doi.org/10.1021/acsaem.2c03689

[48] Yang, Y.;Pang, D.;Wang, C.;Fu, Z.;Liu, N.;Liu, J.;Wu, H.;Jia, B.;Guo, Z.;Fan, X.; Zheng, J. Vacancy and Dopant Co-Constructed Active Microregion in Ru–MoO3−x/Mo2AlB2 for Enhanced Acidic Hydrogen Evolution. Angew. Chem. Int. Ed. 2025, 64.
https://doi.org/10.1002/anie.202504084

[49] Qiu, L.;Tian, F.;He, L.;Li, M.;Lin, F.;Li, L.;Ren, X.;Wu, F.;Li, L.;Zhang, T.;Sheng, J.;Yu, Y.;Yang, W.; Guo, S. Robust Interfacial Hydrogen-Bond Network on Positively Charged Ru-N-Ni Dual Sites Boosts Alkaline Hydrogen Electrocatalysis. Adv. Mater. 2025, 22, e12568.
https://doi.org/10.1002/adma.202512568

[50] Hou, L.;Li, Z.;Jang, H.;Kim, M. G.;Cho, J.;Zhong, W.;Liu, S.; Liu, X. Partially Interstitial Silicon-Implanted Ruthenium as an Efficient Electrocatalyst for Alkaline Hydrogen Evolution. Angew. Chem. Int. Ed. 2025, 64, e202423756.
https://doi.org/10.1002/anie.202423756

[51] Zhao, K.;Xiang, N.;Wang, Y.-Q.;Ye, J.;Jin, Z.;Fu, L.;Chang, X.;Wang, D.;Xiao, H.; Xu, B. A molecular design strategy to enhance hydrogen evolution on platinum electrocatalysts. Nat. Energy 2025, 10, 725-736.
https://doi.org/10.1038/s41560-025-01754-4

[52] Li, R.;Zhao, H.;Wang, L.;Zhou, Q.;Yang, X.;Jiang, L.;Luo, X.;Yu, J.;Wei, J.; Mu, S. Strengthened d–p orbital hybridization and hydrogen diffusion in a hollow N-doped porous carbon/Ru cluster catalyst system for hydrogen evolution reactions. Chem. Sci. 2025, 16, 4383-4391.
https://doi.org/10.1039/D4SC08498E

[53] Qin, Q.;Jang, H.;Jiang, X.;Wang, L.;Wang, X.;Kim, M. G.;Liu, S.;Liu, X.; Cho, J. Constructing Interfacial Oxygen Vacancy and Ruthenium Lewis Acid–Base Pairs to Boost the Alkaline Hydrogen Evolution Reaction Kinetics. Angew. Chem. Int. Ed. 2023, 63, e202317622.
https://doi.org/10.1002/anie.202317622

[54] Jiang, Y.;Qiu, P.;Liu, Q.;Li, P.; Chen, S. Electric-Double-Layer Mechanism of Surface Oxophilicity in Regulating the Alkaline Hydrogen Electrocatalytic Kinetics. J. Am. Chem. Soc. 2025, 147, 14122-14130.
https://doi.org/10.1021/jacs.4c14511

[55] Xu, P.;von Rueden, A. D.;Schimmenti, R.;Mavrikakis, M.; Suntivich, J. Optical method for quantifying the potential of zero charge at the platinum–water electrochemical interface. Nat. Mater. 2023, 22, 503-510.
https://doi.org/10.1038/s41563-023-01474-8

[56] Jin, H.;Chen, X.;Da, Y.;Fan, L.;Jiang, R.;Xiao, Y.;Yao, B.;He, Q.;Yu, Y.; Chen, W. Identifying the Bifunctional Mechanism in Alkaline Water Electrolysis by Lewis Pairs at the Single-Atom Scale. J. Am. Chem. Soc. 2025, 147, 3874-3884.
https://doi.org/10.1021/jacs.4c18040

[57] Yang, Y.;Dong, M.;Wu, Q.;Qin, C.;Chen, W.;Geng, Y.;Wu, S.;Sun, C.;Shao, K.;Su, Z.; Wang, X. In-Situ Growth of Metallocluster Inside Heterometal-Organic Cage to Switch Electron Transfer for Targeted CO2 Photoreduction. Angew. Chem. Int. Ed. 2025, 64, e202423018.
https://doi.org/10.1002/anie.202423018

[58] Zhang, J.;Wan, Z.;Bu, X.;Fan, H.;Lou, H.;Gao, J.;Wen, D.; Gao, W. Electronic Interaction Enables Pt Nanoparticles on N-Doped Porous Carbon Aerogel as Efficient Electrocatalysts for Alkaline Hydrogen Evolution Reaction. Small 2025, 21, e06453.
https://doi.org/10.1002/smll.202506453

[59] Fan, H.;Wan, X.;Sun, S.;Zhou, X.;Bu, X.;Ye, J.;Bai, R.;Lou, H.;Chen, Y.;Gao, J.;Zhang, J.;Gao, W.; Wen, D. Revealing the Role of Ru-O-Ce Interface Coupling in CeO2-Ru Aerogel for Boosting Hydrogen Evolution Kinetics. Adv. Energy Mater. 2025, 15, 2405681.
https://doi.org/10.1002/aenm.202405681

[60] Cui, W. G.;Ren, X.;Wang, S.;Zhang, Y.;Li, Z.;Wang, K.;Gao, F.;Shen, Z.;Liu, Y.;Wang, X.;Wu, Z.;Yang, Y.;Wang, D.; Pan, H. Modulating the Structure of Interfacial Water via Oxygen-Coordinated Tungsten Single-Atom on Nickel Sulfide Slab to Boost Alkaline Hydrogen Evolution. Adv. Energy Mater. 2025, 1, e03257.
https://doi.org/10.1002/aenm.202503257

[61] Li, P.;Jiang, Y.-L.;Men, Y.;Jiao, Y.-Z.; Chen, S. Kinetic cation effect in alkaline hydrogen electrocatalysis and double layer proton transfer. Nat. Commun. 2025, 16, 1844.
https://doi.org/10.1038/s41467-025-56966-9

[62] Li, Z.;Lin, Y.;Garaga, M. N.;Greenbaum, S. G.;Liao, M.;Ruan, J.;Li, Q.;Li, Y.;Sun, D.;Xu, K.;Fang, F.; Wang, F. Quantitative and mechanistic insights into proton dynamics for fast energy storage. Nat. Mater. 2025, 10.1038/s41563-025-02366-9.

[63] Wu, B.;Qi, K.;Petit, T.;Zhang, F.;Xu, Z. J.; Fu, H. Modulation of Interfacial Water at Gas–Liquid–Solid Interface for Water Electrolysis. Angew. Chem. Int. Ed. 2025, 1, e202507327.

[64] Li, C.-Y.;Le, J.-B.;Wang, Y.-H.;Chen, S.;Yang, Z.-L.;Li, J.-F.;Cheng, J.; Tian, Z.-Q. In situ probing electrified interfacial water structures at atomically flat surfaces. Nat. Mater. 2019, 18, 697-701.
https://doi.org/10.1038/s41563-019-0356-x

[65] Yang, C.;Gao, Y.;Xing, Z.;Shu, X.;Zhuang, Z.;Wang, Y.;Zheng, Y.;Li, S.;Cheng, C.;Wang, D.; Zhang, J. Bioinspired Sulfo oxygen bridges optimize interfacial water structure for enhanced hydrogen oxidation and evolution reactions. Nat. Commun. 2025, 16, 6459.
https://doi.org/10.1038/s41467-025-61871-2

[66] Yue, K.;Lu, R.;Gao, M.; Song, F. Polyoxometalated metal-organic framework superstructure for stable water oxidation. Science 2025, 388, 430-436.
https://doi.org/10.1126/science.ads1466

[67] Li, L.-J.;He, Y.;Yang, Y.;Guo, J.;Lu, Z.;Wang, C.;Zhu, S.; Zhu, S.-F. Recent Advances in Mn, Fe, Co, and Ni-Catalyzed Organic Reactions. CCS Chem. 2024, 6, 537-584.
https://doi.org/10.31635/ccschem.023.202303412

[68] Dong, H.;Jiang, J.;Xie, S.;Lin, C.;Wei, P.;Zhang, X.;Hu, P.;Iwuoha, E. I.; Peng, X. Transition metal phosphides for efficient hydrogen evolution: Synthesis, multiscale regulation, and industrial prospects. Appl. Energy 2025, 400, 126550.
https://doi.org/10.1016/j.apenergy.2025.126550

[69] Liu, G.;Ding, L.;Meng, Y.;Ali, A.;Zuo, G.;Meng, X.;Chang, K.;Li, O. L.; Ye, J. A review on ultra-small undoped MoS2 as advanced catalysts for renewable fuel production. Carbon Energy 2024, 6, e521.
https://doi.org/10.1002/cey2.521

[70] Pi, C.;Li, X.;Zhang, X.;Song, H.;Zheng, Y.;Gao, B.;Kızılaslan, A.;Chu, P. K.; Huo, K. In-Plane Mott–Schottky Effects Enabling Efficient Hydrogen Evolution from Mo5N6-MoS2 Heterojunction Nanosheets in Universal-pH Electrolytes. Small 2022, 18, 2201137.
https://doi.org/10.1002/smll.202201137

[71] Wan, R.;Yuan, T.;Wang, L.;Li, B.;Liu, M.; Zhao, B. Earth-abundant electrocatalysts for acidic oxygen evolution. Nat. Catal. 2024, 7, 1288-1304.
https://doi.org/10.1038/s41929-024-01266-6

[72] Li, Z.;Li, B.;Yu, M.;Yu, C.; Shen, P. Amorphous metallic ultrathin nanostructures: A latent ultra-high-density atomic-level catalyst for electrochemical energy conversion. Int. J. Hydrogen Energy 2022, 47, 26956-26977.
https://doi.org/10.1016/j.ijhydene.2022.06.049

[73] Lu, X.;Yan, K.;Yu, Z.;Wang, J.;Liu, R.;Zhang, R.;Qiao, Y.; Xiong, J. Transition metal phosphides: synthesis nanoarchitectonics, catalytic properties, and biomass conversion applications. ChemSusChem 2024, 17, e202301687. https://doi.org/10.1002/cssc.202301687

[74] Liu, X.;He, Z.;Ajmal, M.;Shi, C.;Gao, R.;Pan, L.;Huang, Z.-F.;Zhang, X.; Zou, J.-J. Recent Advances in the Comprehension and Regulation of Lattice Oxygen Oxidation Mechanism in Oxygen Evolution Reaction. Trans. Tianjin Univ. 2023, 29, 247-253. https://doi.org/10.1007/s12209-023-00364-z

[75] Hu, E.;Feng, Y.;Nai, J.;Zhao, D.;Hu, Y.; Lou, X. W. Construction of hierarchical Ni–Co–P hollow nanobricks with oriented nanosheets for efficient overall water splitting. Energy Environ. Sci. 2018, 11, 872-880. https://doi.org/10.1039/C8EE00076J

[76] Roy, A.;Kumar, S.;Guilherme Buzanich, A.;Prinz, C.;Götz, E.;Retzmann, A.;Hickel, T.;Bhattacharya, B.; Emmerling, F. Synergistic Catalytic Sites in High-Entropy Metal Hydroxide Organic Framework for Oxygen Evolution Reaction. Adv. Mater. 2024, 36, 2408114. https://doi.org/10.1002/adma.202408114

[77] Yao, Y.;Zhao, G.;Guo, X.;Xiong, P.;Xu, Z.;Zhang, L.;Chen, C.;Xu, C.;Wu, T.-S.;Soo, Y.-L.;Cui, Z.;Li, M. M.-J.; Zhu, Y. Facet-Dependent Surface Restructuring on Nickel (Oxy)hydroxides: A Self-Activation Process for Enhanced Oxygen Evolution Reaction. J. Am. Chem. Soc. 2024, 146, 15219-15229. https://doi.org/10.1021/jacs.4c02292

[78] Qian, Z.-X.;Liang, G.-H.;Shen, L.-F.;Zhang, G.;Zheng, S.;Tian, J.-H.;Li, J.-F.; Zhang, H. Phase Engineering Facilitates O–O Coupling via Lattice Oxygen Mechanism for Enhanced Oxygen Evolution on Nickel–Iron Phosphide. J. Am. Chem. Soc. 2024, 147, 1334-1343. https://doi.org/10.1021/jacs.4c15847

[79] Wang, X.;Zhong, H.;Xi, S.;Lee, W. S. V.; Xue, J. Understanding of Oxygen Redox in the Oxygen Evolution Reaction. Adv. Mater. 2022, 34, 2107956. https://doi.org/10.1002/adma.202107956

[80] Zhang, T.;Zhao, H.-F.;Chen, Z.-J.;Yang, Q.;Gao, N.;Li, L.;Luo, N.;Zheng, J.;Bao, S.-D.;Peng, J.;Peng, X.;Liu, X.-W.; Yu, H.-B. High-entropy alloy enables multi-path electron synergism and lattice oxygen activation for enhanced oxygen evolution activity. Nat. Commun. 2025, 16, 3327. https://doi.org/10.1038/s41467-025-58648-y

[81] Li, L.;Lin, C.;Ma, X.;Ma, Y.;Zhu, A.;Xie, Z.; Zhang, Q. Rational design of membrane electrode assembly for durable anion exchange membrane water electrolysis. Chem. Eng. J. 2025, 508, 160916. https://doi.org/10.1016/j.cej.2025.160916

[82] Zhou, W.;Huang, Y.;Cai, H.;Wang, T.;Li, H.;Zhang, C.;Zhao, L.;Chen, L.;Liao, M.;Tang, Z.;Chen, K.;Gu, J.;Gao, W.;Fan, Z.; Wen, Z. A Strongly Coupled Cluster Heterostructure with Pt–N-Mo Bonding for Durable and Efficient H2 Evolution in Anion-Exchange Membrane Water Electrolyzers. Nano-Micro Lett. 2025, 17, 296. https://doi.org/10.1007/s40820-025-01798-x

[83] Fan, S.;Yao, R.;Niu, Y.;Yao, J.;Sun, Y.;Li, J.; Liu, G. Ultralow-loading Ru clusters on S-doped Co3O4 for synergistic multi-site electrocatalysis toward industrial-current AEMWE hydrogen evolution. Appl. Catal. B: Environ. 2026, 382, 126023. https://doi.org/10.1016/j.apcatb.2025.126023

[84] Shirwalkar, A.;Kaur, M.;Zhong, S.;Pupucevski, M.;Hu, K.;Yan, Y.;Lattimer, J.; McKone, J. Comparing Intrinsic Catalytic Activity and Practical Performance of Ni- and Pt-Based Alkaline Anion Exchange Membrane Water Electrolyzer Cathodes. ACS Energy Lett. 2025, 10, 1779-1785. https://doi.org/10.1021/acsenergylett.5c00439

[85] Guo, D.;Shi, Z.;El-Demellawi, J. K.;Wahyudi, W.;Arsalan, M.;Zhang, H.; Alshareef, H. N. Lithium Metal Batteries for High Temperature Environments. Adv. Energy Mater. 2025, 1, e02943. https://doi.org/10.1002/aenm.202502943

[86] Xiao, X.;Li, Z.;Xiong, Y.; Yang, Y.-W. IrMo Nanocluster-Doped Porous Carbon Electrocatalysts Derived from Cucurbit[6]uril Boost Efficient Alkaline Hydrogen Evolution. J. Am. Chem. Soc. 2023, 145, 16548-16556. https://doi.org/10.1021/jacs.3c03489

[87] Li, S.;Liu, W.;Shi, Y.;Wang, T.;Liu, T.;Xue, X.;Li, R.;Qiao, M.;Wu, Z.-Y.; Zhang, W. Ligand-rich oxygen evolution electrocatalysts reconstructed from metal-organic frameworks for anion-exchange membrane water electrolysis. Sci. Bull. 2025, 70, 1976-1985. https://doi.org/10.1016/j.scib.2025.04.037

[88] Huang, J.;Wang, H.;Huang, X.;Wang, L.;Chang, Y.;Gao, Y.;Du, Y.; Wang, B. Integrating Machine Learning Insights in Membrane Electrode Assembly for CO2 Electrolysis. Adv. Funct. Mater. 2025, 12, e18997. https://doi.org/10.1002/adfm.202518997

[89] Huang, L.; Qi, R. Electrochemical and operation performance of electrolytic air dehumidification with different catalyst coated membrane methods. Int. J. Green Energy 2022, 20, 934-945. https://doi.org/10.1080/15435075.2022.2126942

[90] Lim, B. H.;Majlan, E. H.;Tajuddin, A.;Husaini, T.;Wan Daud, W. R.;Mohd Radzuan, N. A.; Haque, M. A. Comparison of catalyst-coated membranes and catalyst-coated substrate for PEMFC membrane electrode assembly: A review. Chin. J. Chem. Eng. 2021, 33, 1-16. https://doi.org/10.1016/j.cjche.2020.07.044

[91] Ito, H.;Miyazaki, N.;Sugiyama, S.;Ishida, M.;Nakamura, Y.;Iwasaki, S.;Hasegawa, Y.; Nakano, A. Investigations on electrode configurations for anion exchange membrane electrolysis. J. Appl. Electrochem. 2018, 48, 305-316. https://doi.org/10.1007/s10800-018-1159-5

[92] Baibars, I. O.;Huang, H.;Xiao, Y.;Wang, S.;Nie, Y.;Jia, C.;Dastafkan, K.; Zhao, C. Efficient hydrogen evolution at Ni/CeOx interfaces in anion-exchange membrane water electrolysers. Energy Environ. Sci. 2025, 18, 6248-6259. https://doi.org/10.1039/D4EE06113F

[93] Zhai, T.;Wang, H.;Beaudoin, S. R.;Zhang, R.;Kwak, M.;Hou, S.;Guo, Z.; Boettcher, S. W. Perovskite Catalysts for Pure-Water-Fed Anion-Exchange-Membrane Electrolyzer Anodes: Co-design of Electrically Conductive Nanoparticle Cores and Active Surfaces. J. Am. Chem. Soc. 2025, 147, 15448-15458. https://doi.org/10.1021/jacs.5c01621

[94] Xu, G.;Xing, M.;Qiao, Z.;Han, M.;Wu, Y.;Wang, S.; Cao, D. Constructing Ultra-Stable Electrocatalysts to Achieve Adaptability of Industrial-Level Alkaline Water Electrolyzers for Fluctuating Renewable Energies. Adv. Energy Mater. 2025, 15, 2500926. https://doi.org/10.1002/aenm.202500926

[95] Shen, H.;Gao, F.-Y.;Li, H.;Xu, J.;Jaroniec, M.;Zheng, Y.; Qiao, S.-Z. Durable Anion Exchange Membrane Water Electrolysis in Low-Alkaline Concentration Electrolyte. J. Am. Chem. Soc. 2025, 147, 22677-22685. https://doi.org/10.1021/jacs.5c04194

[96] Miller, H. A. Green hydrogen from anion exchange membrane water electrolysis. Curr. Opin. Electrochem. 2022, 36, 101122. https://doi.org/10.1016/j.coelec.2022.101122

[97] Zhao, J.;Wang, K.;Li, X.;Li, X.;Cui, X.; Zhao, X. Localizing the Long-Range Disorder of Reconstructed Cobalt Oxyhydroxides for Anion Exchange Membrane Water Electrolysis. Angew. Chem. Int. Ed. 2025, 12, e202513592. https://doi.org/10.1002/anie.202513592

[98] Yanagi, R.;Yang, P.;Tricker, A. W.;Chen, Y.;Scott, M. C.;Berlinger, S. A.;Zenyuk, I. V.; Peng, X. Enhancing water and oxygen transport through electrode engineering for AEM water electrolyzers. Joule 2025, 9, 102001. https://doi.org/10.1016/j.joule.2025.102001

[99] Lin, G.;Dong, A.;Li, Z.;Li, W.;Cao, X.;Zhao, Y.;Wang, L.; Sun, L. An Interlayer Anchored NiMo/MoO2 Electrocatalyst for Hydrogen Evolution Reaction in Anion Exchange Membrane Water Electrolysis at High Current Density. Adv. Mater. 2025, 37, 2507525. https://doi.org/10.1002/adma.202507525

[100] Mao, J.;Liang, J.;Li, Y.;Liu, X.;Ma, F.;Liu, S.;Ouyang, H.;Cai, Z.;Wang, T.;Zhao, Y.;Huang, Y.; Li, Q. Electrochemical Lithiation Regulates the Active Hydrogen Supply on Ru–Sn Nanowires for Hydrogen Evolution Toward the High-Performing Anion Exchange Membrane Water Electrolyzer. J. Am. Chem. Soc. 2025, 147, 7711-7720. https://doi.org/10.1021/jacs.4c17373

[101] Ding, S.;Li, Z.;Lin, G.;Ding, Y.;Wang, L.; Sun, L. Post-Selenium-Leaching Induced Fast Micro-Bubble Detachment on Nickel-Iron-Based OER Catalyst for Efficient AEM-WE. Angew. Chem. In. Ed. 2025, 1, e202517132. https://doi.org/10.1002/anie.202517132

[102] Zheng, X.;Zheng, X.;Gao, M.;Liu, Y.;Pan, H.; Sun, W. Platinum-Nickel Oxide Cluster-Cluster Heterostructure Enabling Fast Hydrogen Evolution for Anion Exchange Membrane Water Electrolyzers. Angew. Chem. In. Ed. 2025, 64, e202422062. https://doi.org/10.1002/anie.202422062

[103] Li, S.;Liu, T.;Zhang, W.;Wang, M.;Zhang, H.;Qin, C.;Zhang, L.;Chen, Y.;Jiang, S.;Liu, D.;Liu, X.;Wang, H.;Luo, Q.;Ding, T.; Yao, T. Highly efficient anion exchange membrane water electrolyzers via chromium-doped amorphous electrocatalysts. Nat. Commun. 2024, 15, 3416. https://doi.org/10.1038/s41467-024-47736-0

[104] Wang, H.;Wang, X.;Gao, F.;Chen, J.;Ren, X.;Shen, Z.;Wang, K.;Qi, F.;Liu, Y.;Gao, Y.;Yang, Y.;Wang, D.;Li, Z.;Cui, W.; Pan, H. Synergistic Catalysis of Pt-Based High-Entropy Clusters Coupled with Super-Hydrophilic CeO2 Enables Efficient Anion Exchange Membrane Water Electrolysis. Adv. Mater. 2025, 12, e14269. https://doi.org/10.1002/adma.202514269

[105] Jiang, T.;Jiang, X.;Jiang, C.;Wang, J.;Danlos, Y.;Liu, T.;Deng, C.;Chen, C.;Liao, H.; Kyriakou, V. Novel Fe-Modulating Raney-Ni Electrodes toward High-Efficient and Durable AEM Water Electrolyzer. Adv. Energy Mater. 2025, 1, 2501634. https://doi.org/10.1002/aenm.202501634

[106] Cong, L.;Tang, C.;Li, X.;He, W.;Wang, C.;Angelica, E.; Zhang, Q. Li-Doping and Pyrolysis Engineered Robust Anode for Intermittency-Resilient AEM Electrolysis. Adv. Energy Mater. 2025, 12, e04707. https://doi.org/10.1002/aenm.202504707

[107] Malhotra, D.;Devi, T. A.;Nguyen, T. H.;Dinh, V. A.;Kim, N. H.;Tran, D. T.; Lee, J. H. Realizing tailored catalytic performance on ternary FeP-Ni5P4-CoP in-situ confined Prussian blue analogue framework for anion exchange membrane water electrolysis. J. Colloid Inter. Science 2026, 703, 139276. https://doi.org/10.1016/j.jcis.2025.139276

[108] Zhang, J.;Tu, Y.;Xu, X.;Ke, J.;Zhang, L.;Zhong, C.;Zhang, Y.;Du, L.;Jiang, S. P.;Shao, Z.; Cui, Z. A High-entropy Antiperovskite Nitride Enables Efficient Anion Exchange Membrane Water Electrolysis. Adv. Mater. 2025, 37, 2509042. https://doi.org/10.1002/adma.202509042

[109] Zhang, T.;Lin, S. a.;Liu, H.;Dong, Y.;Kang, X.;Hu, S.;Li, S.;Zhang, Z.;Yu, Q.; Liu, B. An Ionomer-Free Gapless Catalyst-Bridging Membrane Electrode Assembly for High-Performance Pure Water-Fed Anion Exchange Membrane Electrolyzer. Adv. Mater. 2025, 12, e09805. https://doi.org/10.1002/adma.202509805

https://doi.org/10.66000/3110-9772.2025.01.06